Modeling and Control of a Standalone Photovoltaic Using Fuzzy Based Perturb and Observe Maximum Power Point Tracking Controller for Water Pumping Application: (Case Study at Koka, Ethiopia)

Habtamu Berhanu Aklilu

A Thesis Submitted to

The Department of Electrical Power and Control Engineering

School of Electrical Engineering and Computing

Presented in Partial Fulfillment of the Requirement for the Degree of Master's in Electrical Power and Control Engineering (Power)

Office of Graduate Studies

Adama Science and Technology University

June 2023

Adama, Ethiopia

Modeling and Control of a Standalone Photovoltaic Using Fuzzy Based Perturb and Observe Maximum Power Point Tracking Controller for Water Pumping Application: (Case Study at Koka, Ethiopia)

Habtamu Berhanu Aklilu

Advisor: Dr. Tafesse Asrat

A Thesis Submitted to

The Department of Electrical Power and Control Engineering School of Electrical Engineering and Computing

Presented in Partial Fulfillment of the Requirement for the Degree of Master's in Electrical Power and Control Engineering (Power)

Office of Graduate Studies

Adama Science and Technology University

June 2023

Adama, Ethiopia

DECLARATION

I hereby declare that this Master Thesis entitled "Modeling and Control of a Standalone Photovoltaic Using Fuzzy Based Perturb and Observe Maximum Power Point Tracking Controller for Water Pumping Application: (Case Study at Koka, Ethiopia)" is my original work. That is, it has not been submitted for the award of any academic degree, diploma or certificate in any other university. All sources of materials that are used for this thesis have been duly acknowledged through citation.

__________________	_________	_________
Name of the Student	Signature	Date

RECOMMENDATION

I, the advisor of this thesis, hereby certify that I have read the revised version of the thesis entitled "Modeling and Control of a Standalone Photovoltaic Using Fuzzy Based Perturb and Observe Maximum Power Point Tracking Controller for Water Pumping Application: (Case Study at Koka, Ethiopia)" prepared under my guidance by **Habtamu Berhanu Aklilu** submitted in partial fulfillment of the requirements for the degree of Mater's of Science in Power Engineering. Therefore, I recommend the submission of revised version of the thesis to the department following the applicable procedures.

______________	______________	________________
Advisor	Signature	Date

APPROVAL SHEET

I, the advisor of the thesis entitled "Modeling and Control of a Standalone Photovoltaic Using Fuzzy Based Perturb and Observe Maximum Power Point Tracking Controller for Water Pumping Application: (Case Study at Koka, Ethiopia)" and developed by **Habtamu Berhanu Aklilu**, here by certify that the recommendation and suggestions made by the board of examiners are appropriately incorporated into the final version of the thesis.

Advisor	Signature	Date

We, the undersigned, members of the Board of Examiners of the thesis by **Habtamu Berhanu Aklilu** have read and evaluated the thesis entitled "Modeling and Control of a Standalone Photovoltaic Using Fuzzy Based Perturb and Observe Maximum Power Point Tracking Controller for Water Pumping Application: (Case Study at Koka, Ethiopia)" and examined the candidate during open defense. This is, therefore, to certify that the thesis is accepted for partial fulfillment of the requirement of the degree of Master of Science in Power Engineering.

Chairperson	Signature	Date
Internal Examiner	Signature	Date
Eternal Examiner	Signature	Date

Finally, approval and acceptance of the thesis is contingent upon submission of its final copy to the Office of Postgraduate Studies (OPGS) through the Department Graduate Council (DGC) and School Graduate Committee (SGC).

Department Head	Signature	Date
School Dean	Signature	Date
Office of Postgraduate Studies, Dean	Signature	Date

ACKNOWLEDGMENT

I want to start by giving God, the Almighty, praise and thanks for his favors during my research.

My advisor **Dr. Tafesse Asrat** has always provided me with invaluable advice and support, and it gives me great pleasure to convey my sincere gratitude to him. I am very appreciative of the excellent advice, motivation, and suggestions that he has provided me while I have been working on this thesis.

In addition to my advisor, I'd like to thank my friends, especially **Mr. Minyamer Gelawe** and **Mr. Demis Jufare**, for making my study and completion of this thesis at the university so pleasurable and competent. They created an academic and incredibly nice study environment.

Without acknowledging the greatest source of my strength, my family and relatives, for their unending love, support and encouragement, my acknowledgement would fall short. Without you there, it would not have been possible.

TABLE OF CONTENTS

LIST OF FIGURES

LIST OF TABLES

LIST OF ACRONYMS

AC	Alternating Current
CRF	Capital Recovery Factor
DC	Direct Current
FLC	Fuzzy Logic Controller
HOMER	Hybrid optimization model for Renewable Energy
IC	Incremental Conductance
IGBT	Insulated Gate Bipolar Transistor
kW	Kilowatt
LCOE	Levelized Cost of Energy
MATLAB	Matrix Laboratory
MPPT	Maximum Power Point Tracker
NASA	National Aeronautics and Space Administration
O&M	Operation and Maintenance
P&O	Perturb and Observe
PG	Power Generation
PID	Proportional Integral Derivative
PV	Photovoltaic
PWM	Pulse Width Modulation
STC	Standard Test Condition
THD	Total Harmonic Distortion
TNPC	Total Net Present Cost

LIST OF SYMBOLS

a	Diode ideality factor
I_d	Diode saturation current,
I_{pv}	Light generated current of the photovoltaic cell
I_{scn}	Short-circuit current at the nominal condition
N_p	Number of cells connected in parallel
N_s	Number of cells connected in series
R_p	Shunt resistance (Ω)
R_s	Series resistance (Ω)
V_d	The voltage across the diode:
V_{ocn}	Open circuit current at the nominal condition
ΔT	Deviation from the nominal temperature in Kelvin
G	Actual irradiance in W/m^2
g	Gravity
K	Boltzmann constant (1.38×10^{-23}) JK^{-1}
q	Electronic charge (1.602×10^{-19})
Q	Water Discharge Rate
T	Module operating temperature in Kelvin
P	Water Density

ABSTRACT

The need for energy has been growing daily in recent years, and PV has received more attention because this energy source is dependable and extremely efficient. The difficulty in the power system is growing as a result of power fluctuation in the transmission and distribution systems, power quality disturbances, and major blackouts, which can lead to notable differences in voltage and network frequency and instability in the systems. The power supply from Ethiopia's electric utility is also insufficient, which makes it difficult to maintain service continuity for the water pumping in irrigation system at Koka. The standalone PV system control along with system components therefore required. Additionally, the maximum power point tracking (MPPT), PV panel, DC-DC boost converter, inverter, LC filter, and three phase induction motor were taken into account as parts of the PV system. The site that was chosen has a 67.52kWh energy consumption. Thus, CSS-MSP-250W PV panel was selected based on the irrigation system's energy demand. To regulate the imbalance and variation of energy and maintain the DC link voltage at 400V, the PV is controlled using a Fuzzy enhanced P&O MPPT algorithm. The THD analysis has been done with and without LC filter and its result are 13.56% and 53.54% respectively. This show that there is almost 40% minimization of harmonics at the output of inverter. The cost of the equipment employed in the proposed system has also been studied. Accordingly, the net present cost and the cost of energy were $8,201.9 and $0.20/kWh respectively which is, reliable and efficient.

Keywords: *Battery, Converter, Fuzzy Logic Controller, Maximum power point tracking, Microgrid, off-grid, and Photovoltaic*

CHAPTER ONE

INTRODUCTION

1.1. Background of the Study

Our lives and economy depend greatly on energy. The industrial revolution has significantly raised the need for energy. Fossil fuels are beginning to progressively run out. Our civilization is gravely in danger of extinction. On the other hand, traditional energy generation is still contributing to rising greenhouse gas emissions. Reducing carbon dioxide emissions, maintaining reliable, inexpensive energy, and developing more sustainable energy systems are all major worldwide challenges. Renewable energy sources are seen to be the best choice for producing clean, sustainable energy, and solar energy is particularly sustainable and low in carbon emissions. Solar power systems are often used in remote locations where it is impractical to reach the grid supply (D. A. Mousse et al., 2013).

In developing nations, agricultural production and rural water supplies are mostly reliant on rainfall and are negatively impacted if adequate water sources are not available. When there is timely access to sufficient water for irrigation, crop output losses caused by inadequate irrigation facilities can be reduced. Water must therefore be pumped in order to improve agricultural and urban/rural water supplies and lessen reliance on rainfall. In Ethiopia, 85% of the population is rural and relies on low-productivity agriculture. The majority of people live in highland regions. Ethiopia, however, has a large number of rivers and the potential for groundwater. Our nation's farmers will be fruitful if these water resources are extensively utilized for irrigation (U. Report).

The solar-powered water pumps are used to supply water for everything from livestock irrigation to far-flung homes or entire villages. Most PV water pumping systems employ DC motor-driven pumps and are directly connected to the solar panels. Although this system is simple to use, it is inefficient and frequently needs repair. An inverter with an AC motor is used with solar pumps powered by AC drives. Better options are available with an induction motor in terms of size, toughness, efficiency, and maintainability. Recent advancements in low-cost, high-power power electronics have expanded the scope of applications for AC drives. Induction motor drives and power electronic converters have thus taken the position of DC motor drives in irrigation systems (M. Ababa, 2014) (I. Sefa and I. Altin, 2017).

Today, the majority of research is devoted to improving the usage of unconventional energy sources. Solar Photovoltaic (PV) technology is one of the most widely used non-conventional energy sources since it provides so many benefits. When compared to conventional energy sources, solar photovoltaic panels have a number of advantages, including the ability to absorb free, perpetual solar energy, their environmental friendliness (they don't release any pollution into the atmosphere), and their low maintenance requirements. According to (I. Sefa et al., 2015) and (J. S. Lai et al., 2013), it converts solar energy from the Sun directly into DC electric power.

Choosing the right site to conduct the study is essential. Site selection is crucial for a sustainable water supply plan, however, when sizing PV water pumping systems, many designers usually undervalue its significance. Without a dependable water source, installing the greatest system is a waste of money. The amount of water needed for the proposed uses, as well as the type, quantity, and quality of available water resources, were taken into consideration when choosing the research site. Koka in Adama, which lies in the southern portion of Ethiopia, was chosen for this investigation based on these features.

The change in radiation during the day makes it challenging to control the most optimal solar energy. This research thesis is studied the water pump load based on the size of the motor and the area of the land. In addition to PV solar, MPPT, inverter, DC to DC, LC filter, and three phase induction motor are examined. Under variable irradiance conditions, a comparison analysis of the traditional P&O and a fuzz logic-based P&O controller is investigated. An AC motor will be utilized to pump the water in the irrigation system to increase reliability. As a result, it can reduce operating and maintenance expenses. The design and analysis of a solar-powered feed induction motor drive for a water pumping system for a farm irrigation application are done using the MATLAB software in this study.

1.2. Statement of the Problem

Conventional techniques, such as diesel-powered generators and direct-coupled DC motors, have been employed in the proposed application for decades. Diesel pumps and DC motors have a number of problems, including high operating and maintenance costs, erratic fuel availability, and a limited supply of spare parts. One renewable energy source that doesn't cause air pollution is solar. But, the fundamental goal and challenge in modeling solar power plants is to extract the maximum possible output power while taking certain variable factors, like irradiance, into consideration. The current state of research demonstrates the widespread use of P&O and other MPPT controller approaches. These methods can, however, make reference to the local maximum found in the PV characteristics. Intelligent controllers, such as fuzzy logic, can change the output power to the load's ideal level at the global maximum. In this study, a Fuzzy enhanced P&O MPPT algorithm has been employed.

Induction motor is considered as a drive for water pumping this is because it operates reliably and with less maintenance. This is due to the fact that it doesn't require replacing brushes like DC motors do. To drive an induction motor with the necessary voltage, a boost DC-to-DC converter and a three-phase inverter are utilized. However, a conventional two-level inverter may generate harmonics in the output current and it may lead to degradation of equipments. Therefore, a low pass LC filter is designed to have less harmonics. To confirm the suggested solar energy controller results and the performance of the traditional P&O controller, a comparison result analysis is conducted. Moreover, the output current with and without filter is analyzed.

1.3. Objectives of the Study

1.3.1. General Objective

The main objective of this thesis is modeling, analysis, and control of standalone photovoltaic energy system for water pumping application system using fuzzy based P&O controller under variable irradiation condition.

1.3.2. Specific Objectives

The specific objectives of this thesis are to:

- To determine the power demand of the selected area.
- To estimate and select the size of the PV panel, DC-DC converter, and inverter.
- To develop output power control of PV using fuzzy based P&O MPPT controller.
- To reduce the THD value of the two level three phase inverter using filter design.
- To extract the optimal output power under variable irradiation conditions.

1.4. Scope of the Study

The deficit in electricity and high diesel costs affects the pumping requirements of community water supplies and irrigation. Therefore, using solar energy for water pumping is a promising alternative to conventional electricity and diesel-based pumping systems. The scope of this thesis is modeling and control of solar powered water pumping system using fuzzy-based P&O controller for farm irrigation using MATLAB/Simulink.

1.5. Limitation of The Study

This research work is limited to the simulation of the system using MATLAB/Simulink software by showing how the different components of the system interact with each other. The reason behind this is the implementation of a real system, which is difficult to procure the components. Along with it takes the additional time and cost incurred in making the actual prototype implementation.

1.6. Significance of the Study

The purpose of this research is to present the benefits of replacing diesel water pumping system by photovoltaic water pumping system in farm irrigation. The benefit will be demonstrated in terms of environmental perspectives to show how much reduction in CO_2 emissions is when using photovoltaic system. The wastage of energy and air pollution are the major issues in the world as well as our country Ethiopia. Therefore, the world is replacing non-renewable energy source into renewable energy source. Due to the above-mentioned reasons, the renewable energy is accepted in many countries.

1.7. Thesis Organization

There are five chapters in this research thesis.

Introduction to the research project, problem description, research questions, objectives, scope, restrictions, motivation, and importance of the research thesis are presented in Chapter-1. Chapter-2 explains thesis's theoretical foundation and related works. The methodologies used for this study and mathematical modeling of the system are described in Chapter 3. Chapter-4 demonstrates the result and discussion parts of the work. The intended results and debates are presented in Chapter-5. Chapter-6 discusses the conclusion and suggestions for further work.

CHAPTER TWO

THEORETICAL BACKGROUND AND LITERATURE REVIEW

2.1. Chapter Overview

The overall thesis theory and notion is covered in this chapter. In order to categorize how much this thesis relates to previous study and theory, it is important to explain the viewpoint and methodology that were used in the earlier studies. The idea and concept used to solve the problem are demonstrated in this chapter. In order to do any form of research, theoretical understanding is crucial. Ethiopia uses a lot of electrical and diesel-powered water pumping devices for irrigation purposes.

2.2. Renewable Energy

Although fossil fuels are still widely used today, they are being depleted by humanity far more quickly than they are replenished by natural resources. Fossil fuels are therefore considered non-renewable at the current pace of consumption (V. Quaschning, 2010). Because of this, recent research revealed that the demand for renewable energy sources is currently a major concern. Today, solar energy and its main and secondary effects on the earth are closely related to renewable energy sources.

Solar radiation, wind, water, and specific types of flora and biomass all have an impact on the environment. Additionally, geothermal forces (such as the heat of the planet's core) and gravitational forces (such as tides) are linked to renewable energy sources. Renewable energy sources are known to replenish themselves over the duration of a person's lifetime and can be used in conjunction with the necessary technological apparatus to produce predictable amounts of energy when required. In addition, compared to other resources like fossil fuels and nuclear power, renewable energy systems seem to be more evenly distributed throughout the world (Benghanem, M. and e. al.,2013).

Currently, 13.6 percent of the world's energy consumption is attributed to renewable energy sources. Furthermore, it is anticipated that by 2040, renewable energy sources will provide roughly 47.7% of the world's energy consumption. The contribution that renewable energy sources provide to the decrease of environmental pollution and the potential for its complete removal on a large scale is one of its most important benefits (V. Quaschning, 2010).

2.2.1. Renewable Energy Scenario in Ethiopia

Ethiopia's strong GDP growth over the preceding ten years has led to a steady rise in the country's need for power. It is possible to produce more than 60,000 megawatts (MW) of electricity using renewable energy sources, including hydroelectric, wind, sun, and geothermal. The potential of Ethiopia's energy resources is displayed in Table 2.1 (EEP, 2016).

Table 2.1. Energy resource potential of Ethiopia (EEP, 2016)

Resource	Exploitable Reserve	Exploited Percent
Agricultural Waste	15-20 million tons	30%
Coal	300 million tons	0%
Geothermal	<10,000 MW	<1%
Hydropower	45,000 MW	<5%
Oil Shale	253 million tons	0%
Natural Gas	112 billion m3	0%
Solar/day	4-6 kWh/m2	<1%
Wood	1120 million tons	50%
Wind: Power Speed	100>7 GW m/s	<1%

Source: Ethiopian Electrical Power (December 2016)

2.3. Photovoltaic System

Due to its noiseless operation and compact size, the photovoltaic system is a desirable renewable energy source for distributed energy generating (Panels1, 2023). As a result, solar systems are becoming increasingly popular worldwide. The phrases photo and voltaic, which both refer to the production of voltage and light, are combined to form the word photovoltaic. Consequently, solar energy is turned directly into electrical energy by employing solar cells (Panels2, 2023). When exposed to sunlight, the photovoltaic array generates electricity. The electric power generated by the photovoltaic array must be converted, controlled, conducted, distributed, and stored, which requires a number of interface components.

PV Array: A group of modules in a single system is referred to as an array. A module can be connected in parallel, series, or to reach desired power ratings when the energy produced by the module is insufficient for specific purposes.

PV cell: The building block of photovoltaic systems, photovoltaic cells (also known as solar cells) are covered in a protective laminate to form photovoltaic modules.

PV module: A photovoltaic module, also known as a photovoltaic panel, is a collection of cells. In order to improve the voltage rating of the photovoltaic module or panel, cells are typically connected in series. The photovoltaic structure of PV cells, modules, and arrays is depicted in Figure 2.1.

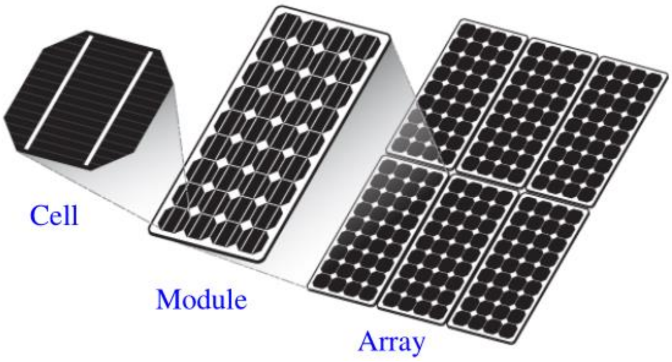

Figure 2.1. Structure of PV cell, module, and array (Panels1, 2018).

2.3.1. Types of solar photovoltaic cells

Different materials are used in the production of photovoltaic cells. A semiconductor called silicon is utilized to build solar panels. Monocrystalline silicon photovoltaic cells, polycrystalline silicon photovoltaic cells, and thin films are the three categories of photovoltaic cell types that predominate the global market. Table 2.2 explains the benefits, drawbacks, and efficiency rates of each type of solar cell.

Table 2.2. Multi-criteria for types of photovoltaic cells (Online1, 2023)

Cell Types	Efficiency	Advantage	Disadvantage
Monocrystalline	20%	Highly efficient, durable	Most expensive
Polycrystalline	15%	Less expensive, improving efficiency	Slightly lower efficiency not as durable
Thin film	7-10%	Low cost and easily produced	Shorter warranties, shorter lifespan

2.3.2. Working Principles of Solar Photovoltaic

When semiconducting materials in the photovoltaic cell are doped a P-N structure of photovoltaic effect is formed. The p-type or positive silicon can give up electrons and get holes while the n-type or negative silicon receives electrons. When cells are hit by sunlight, the photons in light excite a few of the electrons in the semiconductors to form negative-positive or electron-hole pairs and then the electric field is formed. The following Figure 2.2 shows how the photovoltaic solar works.

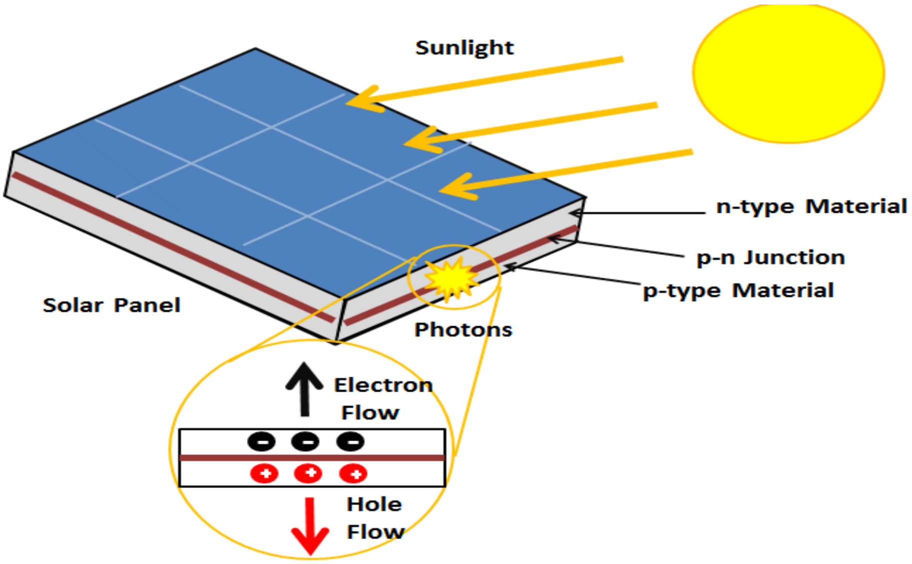

Figure 2.2. How photovoltaic solar works (Online2, 2023).

Positively charged particles are forced to move in the opposite direction by the field that is formed. Since the electron flows to the n-side instead of the p-side, the hole is formed, and the free electron has a tendency to move there. The hole is then travelling to the p-side or away from an electron. In the cell, an electric current is created by the movement of this electron. How the photovoltaic is operated in the solar cell is the name of this procedure.

2.3.3. Electrical Characteristics of Photovoltaic Panel

Most photovoltaic modules are rated with standard test conditions (B. V. Emmanuel, 2009). Standard test conditions have the following factors:

Cell temperature: It will be differing from ambient air temperature. Standard test conditions define cell testing temperature as 25^0c (Online 3, 2023).

Irradiance: It is a power or sunlight intensity that is described in watts per square meter falling on a flat surface. The measurement standard is expressed as 1,000 Watts/m^2.

2.3.4. Factors that Affect Reliability and Performance of PV Cell

Solar Cell Conversion Efficiency (η): The efficiency of a PV solar cell is the ratio of the generated maximum output power to the incident or input power (M. Martino, 2012). Some of the output parameters affect how efficient a solar PV cell is and they are defined as follows (M. Martino, 2012).

$$\eta = \frac{V_{oc} \times I_{sc} \times FF}{P_{in}} \tag{2.1}$$

where: FF = the fill factor. I_{sc} = the short circuit current, P_{in} = the incident light power on the device, and V_{oc} = open circuit voltage,

Short Circuit Current: The short-circuit current is results from short-circuiting the cell's negative and positive terminals. In addition, the voltage between the terminals is zero, which equates to no load resistance (M. Martino, 2012). It is based on the incident light's spectrum and photon flux density.

Open Circuit Voltage: In open-circuit voltage, a load is not connected to the solar PV cell terminals. It is the highest voltage that a photovoltaic solar cell is capable of producing in any lighting condition. The greatest voltage when no current is flowing through the external circuit is known as the open-circuit voltage.

Fill factor: Fill factor (FF) is one of the key characteristics of a solar photovoltaic module's efficiency. On the current vs voltage curve of the solar photovoltaic module, the fill factor must be as high as possible and close to unity in order to achieve the highest efficiency. The fill factor value, on the other hand, provides a clue of the PV array's quality; the closer it is to one, the more electricity the array can produce (D. K. Sharma, 2014). The value of FF drops as a result of parasitic components being present in the solar cell. As a result, the fill factor values range from 0.7 to 0.8. It can be mathematically represented as the following relationship between theoretical power and maximum power. I-V Curve with a varying fill factor of solar cell is shown in Figure 2.3.

$$FF = \frac{V_{mp} \; I_{mp}}{V_{oc} \; I_{sc}} \tag{2.2}$$

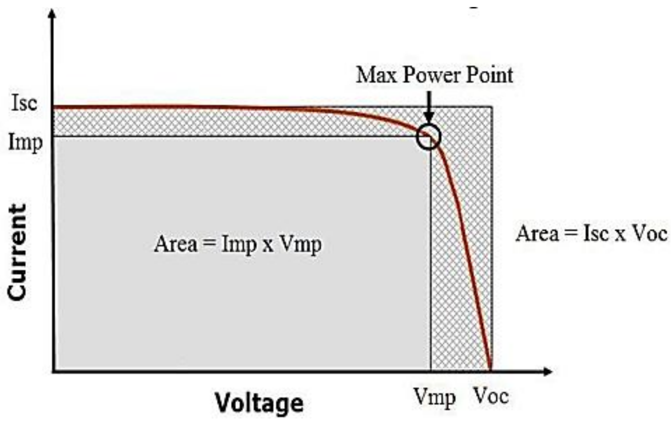

Figure 2.3. I-V Curve with a varying fill factor of solar cell (M. Martino, 2012).

2.3.5. DC to DC Converters

The power electronic circuit that changes a DC voltage from one voltage level to another is known as a DC-DC converter. Different conversion techniques exist, including linear, electrical, magnetic, switched-mode, and capacitive. Switched-mode DC-DC converters are one of them, and they are the circuits that this thesis work describes. When switching direct current electrical power from one voltage level to another is required, this device is employed. Because DC cannot be simply stepped down or up using a transformer, DC-DC converters is particularly crucial. Thus, a transformer is created using a DC -DC converter. Essentially, they do is transform the supplied power into different impedance levels (Online4, 2023). Therefore, regardless of the output voltage levels, power is produced from the input. Different types of DC-DC converters are available and can be used to shift one voltage level to another. Some of them were discussed below.

The buck converter: Depending on its needs, the buck converter is employed in circuits to step down the voltage level from the input voltage. Buck converter is easy and inexpensive. When a buck converter is operating, the switch is initially open, which means that no current is flowing through any section of the circuit. When the switch is closed, however, a gradual buildup of current begins to flow through the inductor. The voltage at the inductor's output is lower than the first when the switch is closed because the inductor pulls current through the diode.

Boost Convertor: A power converter with a higher output DC voltage than its input DC voltage is referred to as a boost converter or step-up converter. The source current is greater than the output current where power must be conserved. The buck converter's components are the same in this converter, but the output voltage is higher than the source voltage.

Buck-Boost Converter: The buck-boost converter is another common switched-mode converter (Online4, 2023). This buck-boost converter will produce an output voltage that is either lower or greater than the input voltage.

2.4. Inverters

Any standalone PV system with ac loads needs inverters, commonly referred to as power conditioning devices. The system's DC operating voltage will be determined in part by the inverter that choose. Both the DC input and the AC output requirements must be taken into account when specifying an inverter (G. E. Ahmad, 2019). Not just how much power the inverter will need, but also what variation in voltage, frequency, and waveform can be handled, should all be taken into account while designing the AC load. The DC voltage, surge capacity, and allowable voltage variation must all be stated for the input side. The optimum inverter for a given application must be chosen after carefully examining many factors. The choice of inverter will affect the performance and reliability of a PV system.

2.4.1. Types of Inverters

Inverters come in two different basic varieties that are frequently used in adjustable AC drive systems. Both are known as current source inverters and voltage source inverters. The square-wave six-step voltage source inverter (VSI), also known as the variable voltage inverter (VVI), receives DC power from a source with adjustable voltage and modifies the frequency and voltage (G. E. Ahmad, 2019). An adjustable current source provides DC power to the current source inverter (CSI), which then modifies the frequency and current. Comparing voltage source inverters versus current source inverters is shown in Table 2.4. Since voltage source inverters (VSI), which include PWM Inverters, are used in this study.

Table 2.3. Comparison between VSI and CSI (G. E. Ahmad, 2019)

Voltage Source Inverter (VSI)	Current Source Inverter (CSI)
Inverter fed by a stiff voltage source	Inverter fed by a stiff current source
DC source has low internal impedance	DC source has high internal impedance
Half bridge, full bridge, square wave and pulse width modulated inverters fall under VSI	Capacitor commutated CSI and auto sequential commutated inverters (ASCI) fall under CSI
Need feedback diodes	No feedback diodes required

2.5. Water Pumps

In order to move or enhance liquids in this case, water between two different sites, pumps use more energy. Typically, these are used in home, commercial, and agricultural applications. The choice of a certain pumping system for a given application is a pretty crucial choice that will be influenced by the required energy demand and discharge, head, performance, and financial costs (Government Printing Office, 2012). The most common forms of pumps are centrifugal pumps and positive displacement pumps, and each is utilized in a particular industry.

2.5.1. Categories of Water Pumps.

Different types of pumps can be utilized for water pumping purposes. They can be divided into groups based on their design (such as rotational or positive displacement pumps), their location (such as surface or submersible pumps), or the motor they utilize (such as AC or DC). For deep wells and huge water demand, centrifugal pumps are typically recommended (Maria Ines Cardoso Bexiga, 2014). Displacement pumps are often only used for small volumes.

Selection of Piping Material: The following factors need to be taken into account while choosing piping materials (Benghanem, M. and e. al, 2013). The pipe must be cost-effective, have adequate corrosion resistance, and satisfy the mechanical requirements of the system. Polyvinyl chloride (PVC) piping is the most frequently used material for water pumping applications, according to the various piping handbook (McGraw-Hill), because of its many benefits, including good chemical resistance and favorable operating pressure ratings.

2.5.2. Motor Based PV Pumping System

Several types of electric motors are currently used in water-pumping applications. The squirrel-cage induction motor is the most basic form of AC motor. It is the most widely used motor for wind/PV systems due to its low cost and rugged design. The PV array, DC-DC converter, inverter, induction motor, and water pump make up the three-phase water pumping system. The DC-DC converter which is coupled to the inverter to convert the DC power to variable voltage for the induction motor, as the AC pumping motor cannot be attached directly to the PV cells (E. Muliadi, 1997).

2.5.3. AC Motor

In an induction motor, the magnetic flux in the rotor is produced by the magnetic field of the stator winding, which induces the flux. A comparison has been made in Table 2.6.

Table 2.6 Comparing AC motor and DC motor

Basics	AC Motors	DC Motors
Input	AC voltage.	DC voltage.
Supply phase	Single phase and three phase.	Only single-phase supply is used.
Armatures	Armatures does not rotate.	Armature rotates.
cost	Repairing is not costly.	Repairing DC motor is costly.
brushes	Does not use carbon brushes.	DC motor uses carbon brushes.
Life spam	It has longer life spam.	It has less life spam.
Commutation	No commutation processes.	There is commutation process.

2.5.4. PV Water Pumping Storage

Water is only delivered by direct-coupled PV pumps when the sun is shining. In order to meet the need when the sun is not shining, this might necessitate some sort of water storage. Installing 3 to 10 days' worth of water storage is typically easier and more cost-effective than storing power in batteries. The storage canal is a location where elevated water is kept in order to create pressure at the exit that is at ground level. If the crop needs water, the water in this system is used to feed the plants at night and during cloudy weather (Maria Ines Cardoso Bexiga, 2014).

2.6. Related Works

In his section, other related previous works are reviewed and the gap between previews work and this work is discussed briefly.

Design, simulation and analysis of photovoltaic water pumping system for irrigation of a potato farm at Gerenbo southern Ethiopia in literature **(**J. S. Lai et al., 2013**)** (H. Mark, 2010)**.** This paper aims to present the benefits of replacing diesel water pumping system by photovoltaic water pumping system in irrigation of a potato farm using river (surface) water available in the area. The finding of this research shows us using solar power for the water pumping system is a good opportunity in terms of solar availability, carbon emission control and economically effective.

Study of PV based water pumping system for agricultural sector aiming to evaluate ways of efficient PV powered water pumping system is discussed in literature (M. Parimita et al., 2016). Photovoltaic-battery hybrid system feds the vector control of an asynchronous motor, PV generator, converter of DC-DC, battery, converter of DC-AC, an induction motor controlled by a vector and the centrifugal pump are investigated in this paper.

This paper presents the effect of pumping head on solar water pumping system in literature (Guide, 2018). The aim of this work is to determine the effect of pumping head on PVWPS using the optimum PV array configuration, adequate to supply a DC Helical pump with an optimum energy amount, under the outdoor conditions of Madinah site. Four different pumping head have been tested (50 m, 60 m, 70 m and 80 m). The tests have been carried for different heads, under sunny daylight hours, in a real well at a farm in Madinah site. The flow rate Q depends basically on two factors: the pumping head H and the global solar irradiation Hg.

Study a review of solar-powered water pumping systems comparing to diesel powered pumping system in different countries is presented in literature (US, 2012). The result of this research paper shows, almost all the installed solar-powered water pumping systems heads do not exceed 200m, since as increase in system head there is increase in power supply, and this system are more economical at low pumping capacities compared to diesel and wind-powered water pumping systems. A solar-powered water pumping system contributes to a clean environment by reducing the carbon emission compared to other power supply system.

This paper presents the viability of the solar/ wind and hybrid water pumping system for off-grid rural areas in Ethiopia in literature (E. Muliadi, 1997) (H. Mark, 2010)**.** This can be achieved by studying Solar and Wind Potential at the selected site and design a water pumping system for both solar and wind and by combining the two-energy source solar and wind, the Hybrid water pump has been designed. In this paper maximum power point tracking and energy storage battery was not used. The paper concludes that the Hybrid water pumping system is more feasible than a standalone PV and Windmill.

In all reviewed researches, mostly they used directly coupled PV panel to DC motor Pump has been used but this has its own disadvantages; DC motor has high starting torque which is mismatch with variable load torque, this is due to variable solar irradiances this may cause damage of equipment or not operate properly. DC motor is not available everywhere easily, it is so expensive and also it needs high maintenance. Nowadays, AC motor is more appropriate for water pumping systems, because it has constant torque, less expensive than DC motor, simple, easily maintained, available everywhere and has less efficiency than DC motor pumping. Moreover, technically there are many limitations and drawbacks. The firs limitation is that most of the research are highly implemented using conventional MPPT controllers like P&O. This leads to the output power trucks the local maximum in the PV characteristic curve. The other thing is that the implementation of three phase converter has a significant harmonic. Thus, in this research thesis the overall load is analyzed for the selected area. The solar analysis including the DC-to-DC converter, Inverter, LC filter design and the Fuzzy-P&O output power control system design are done. Its result is highly outperformed the results of a conventional control P&O algorithm.

CHAPTER THREE

METHODOLOGY

3.1. Introduction

This chapter deals with the data collection, designing process of solar powered water pumping system, mathematical modelling for photovoltaic cell, designing and modelling of boost converter, fuzzy based P&O MPPT, and designing of two-level inverter.

3.2. Methodologies

In order to attain the general and specific objectives of this study, the following methods and techniques is followed as shown in Figure 3.1. First the related works are reviewed and then, the necessary data to the research is collected and analyzed. The load demand of the system is determined and PV module is selected. The DC-DC boost converter is designed to get the required output voltage.

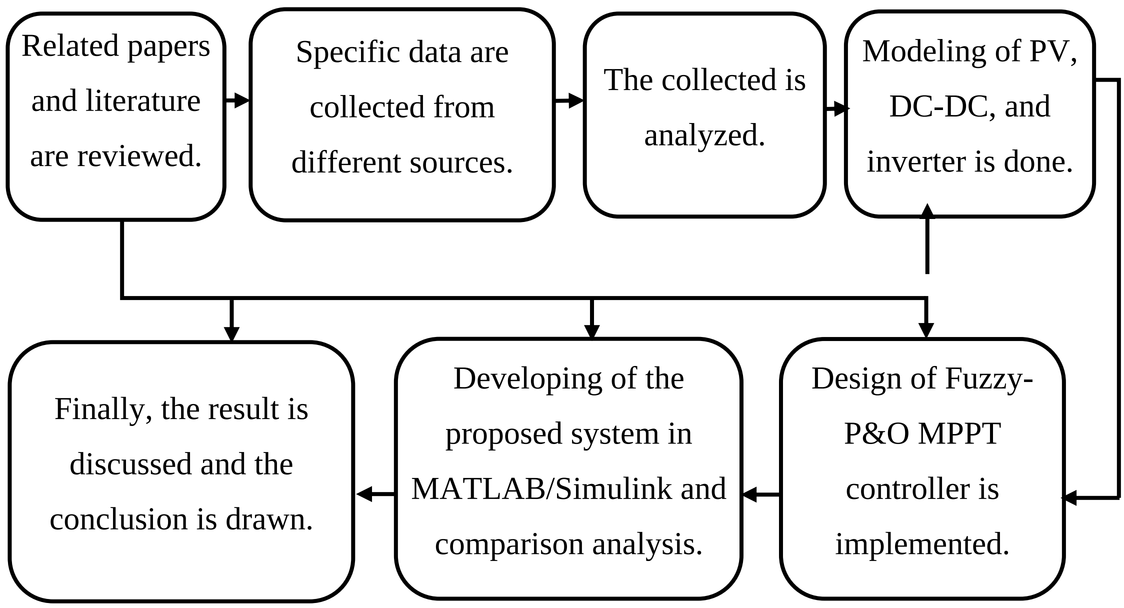

Figure 3.1. Block diagram of the research methodology

A Fuzzy based P&O algorithm is incorporated to get the desired output power. This voltage is given as input to two level inverter which converts the DC to AC voltage and drives induction motor. Finally, the proposed system is developed by using MATLAB/Simulink and the result is discussed and conclusion is drawn.

3.3. Materials

For the system design and editing thesis documentation the following computer software's are used.

- Microsoft office 2019,
- MathType 6.0 equation, and
- MATLAB/2021a

Microsoft office is used for editing the thesis documentation. MathType 6.0 is used for writing mathematical equations in Microsoft office word and Power point presentation tools. MATLAB is used for simulation of the system design.

3.4. System Layout

The layout of the interconnected system is shown in Figure 3.3. The components are solar panel /array, converter (DC to DC and DC to AC converter), pump AC motor, water source, pipelines and tank as shown from the schematic layout of standalone PV system.

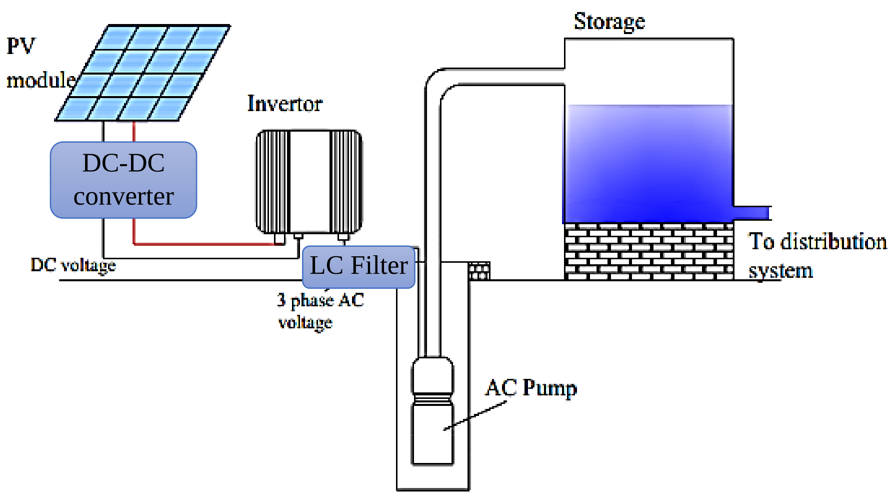

Figure 3.3. Schematic layout of standalone PV system (B. fola, 2020)

3.5. Site Selection

Site selection is vital for a sustainable water supply scheme, yet many designers in sizing PV water pumping systems frequently underestimate its importance. The main criteria for site selection include availability, quality and type of water resource, and the amount of water required for the intended use. This study is done for the case of Koka near to Adama, Ethiopia. Koka is one of the Oromia region's cities in Ethiopia which is located 96km from Addis Ababa. It is found at latitude 8° 26' 13.08" N and longitude 39° 2' 1.44"E at an elevation of 939m / 3081feet that is taken from NASA and google map.

The following Figure 3.2 shows Koka in Oromia reginal state, Ethiopia on google map. Installing the best system without a reliable water source is a waste of financial resources. Similarly, designing a system without estimating the realistic water demand might result in insufficient water supplies or unnecessary financial expenditures for a system that is too large.

Figure 3.2. Koka city, Eastern Shewa, Ethiopia
Source: Google map

When designing a solar water pump system, the water requirement is taken into account to calculate the amount of water. Calculating the typical water needs for the crop cultivated on the land is necessary for this irrigation method. To implement this system, one must be more particular because this requirement varies from place to place. Hence the selected site area is 160,000m^2 (which is almost 400m x 400m). Thus, the flow rate of the water can be determined. To calculate the water flow rate for irrigation, the irrigation water application depth (ET rate) has to be considered and for this study Maize is taken in to account as a main crop for the area and its value is 0.005 m/hr. The volume of water required per hour for the given crop area can be determined as the product of ET rate (m/hr) and Area (m^2) of the site.

Therefore, the water flow rate required for irrigating a 160,000 square meter maize crop with an ET rate of 5mm/hr is 800 cubic meters per hour (m³/hr) or 800,000 L/hr.

3.5.1. Water Source

The primary objective after that is to locate and take into consideration the water supply. It could come from rainwater, surface water, or ground water. The river, borehole, well, pond, and spring are typical sources. The static and dynamic water labels of the source must be examined before determining the water source. The distance from the water's surface to the well's top is static and level. Seasonal changes may be occurring (A. Nasir, 2016).

The difference between the top of the well and the water's surface when the pump is functioning is known as the dynamic level, as opposed to the static level. It can be measured while the pump is running since, typically, it gets smaller. The amount of water may vary depending on the season; thus, some testing or observation must be done to ensure that the dynamic water level remains constant throughout the entire year (A. Nasir, 2016).

3.5.2. Determining Flow Rate for Pump

To evaluate the flow rate of the pump, the flow rate based on the monthly water consumption and the sun's peak hours is considered. The month with the least quantity of insolation has been chosen to ensure that the system is not undersized for any month of the year (Carson Ca, 2011). Based on the expected daily water amount divided by the number of peak sun hours per day, the pump's flow rate analysis is carried out. The average sun hour per day is 5.14, as shown in Table 3.2. Equation (3.1) can be used to compute the pump flow rate design (Carson Ca, 2011) (Shewin Electric, 2009).

$$\text{Flow rate} = \frac{\text{Daily Water Requirement}}{\text{Peak} - \text{Sun Hours}} \tag{3.1}$$

$$\text{Flow rate} = \frac{800,000\text{L}}{5.14\ \text{peak} - \text{Sun Hour} \times 60\ \text{min/ hr}} = 2,594.034\ {}^{\text{L}}\!/_{\text{min}}$$

Hence, in water pumping system for the irrigation the storage of water analysis is necessary. Thus, the storage duration is considered as 8 hours. Then, the capacity of water storage in is 6,400 m³ or (800 m³/hr * 8 hours).

3.5.3. Analysis of Pump Dynamic Head

The primary variable in a water pumping system powered by solar energy is the overall lifting height. This is due to the need to calculate the amount of force required to transfer the water from the well's deep level to the desired location (Shewin Electric, 2009).

$$T_h = f_h + D_h + H_{pipe} + P_h + V_{Rh} + V_h \tag{3.2}$$

Where: f_h is head due to friction loss, D_h is the dynamic head loss, H_{pipe} is the horizontal length of pipe, P_h is pump level head, V_{Rh} is vertical rise head, and V_h is the velocity head.

3.5.3.1. Analysis of Head Loss Due to Friction

The head due to friction loss f_h is calculated by using Darcy-Weisbach formula as in Equation (3.3) (Shewin Electric, 2009).

$$f_h = \frac{fLC^2}{2dg} \tag{3.3}$$

Where L is the pipe's length, g is gravity, d is the pipe's diameter, f is the friction factor, and C is the fluid's mean velocity. However, it is too difficult or challenging to determine the friction factor. The Blasius equation is appropriate for smooth flow and smooth pipes (Carson Ca, 2011) (Shewin Electric, 2009).

$$f = \frac{1.325}{\left[\ln\left(\frac{e}{3.7d} + \frac{5.74}{R_e^{0.9}}\right)\right]^2} \tag{3.4}$$

Reynolds' coefficient Re is obtained as,

$$R_e = \frac{\rho V d}{\mu} \tag{3.5}$$

The formula for calculating a fluid's average velocity, V, is

$$V = \frac{Q}{A} \tag{3.6}$$

where Q is the water discharge rate, A is the pipe's area, and it is determined by $\pi * d^2/4$.

$$V = \frac{4*Q}{\pi * d^2} \tag{3.7}$$

Then, it can be calculated as,

$$V = \frac{4 * 0.0043 m^3 / \sec}{\pi * 0.05^2 m^2} = 2.2 m / \sec$$

Now that the Reynolds value has been calculated using Equation (3.5),

$$R_e = \frac{\rho V d}{\mu} = \frac{1000 Kg / m^3 * 2.2 m / \sec * 0.05 m}{1.14 * 10^{-3} Ns / m^2} = 96,491$$

where μ is the dynamic viscosity, ρ is the water density, and R_e is the Reynolds number. The type of flow depends on R_e's value (Carson Ca, 2011) (Shewin Electric, 2009).

- If $R_e < 2000$, the flow is called laminar.
- If $R_e > 4000$, the flow is called turbulent.
- If $2000 < R_e < 4000$, the flow is transition.

Since in this system $R_e > 4000$, the flow is turbulent. Table 3.1 shows common pipe materials.

Table 3.1. Common pipe materials (Carson Ca, 2011) (Shewin Electric, 2009)

Material	Roughness(ft)
Asphalted cast iron	0.004000
Commercial steel	0.000150
Drawn bass or copper	0.000005
Galvanized iron	0.000500
PVC pipe	0.000005
Wrought iron	0.000150

For PVC, $\varepsilon \approx 1.5 * 10^{-6} m$, the relative roughness is:

$$\gamma = \frac{\varepsilon}{d} = \frac{1.5 * 10^{-6} m}{0.05 m} = 3 * 10^{-5} \tag{3.8}$$

Since, $R_e > 4000$, applying the above Equation (3.4) the friction factor is determined as shown below.

$$f = \frac{1.325}{\left[\ln \left(\frac{e}{3.7d} + \frac{5.74}{R_e^{0.9}} \right) \right]^2} = 0.021$$

Therefore, by applying Equation (3.3) the head loss due to friction f_h is determined as;

$$f_h = \frac{fLV^2}{2dg} = \frac{0.021*100*2.2^2}{2*0.05*9.81} = 10.4m$$

3.5.3.2. Analysis of Dynamic Head Loss

Using Darcy Weisbach equation (Carson Ca, 2011), the dynamic head loss is given by:

$$D_h = K\frac{V^2}{2g} \quad (3.9)$$

Where: K is the combinations of the pipe (straight length) and fittings (bends) gain values.

$$K = K_{pipe} + K_{fitting} \quad (3.10)$$

K_{pipe} is associated the straight length of the pipe used in the system defined as:

$$K_{pipe} = \frac{fL}{d} = \frac{0.021*100}{0.05} = 42 \quad (3.11)$$

$K_{fitting}$ refers to fittings used in the pipe that carries water from the receiving tank to the surface. It can be found by adding the individual fitting values from the standard tables to determine the overall $K_{fitting}$ values. The $K_{fitting}$ calculation for the system under consideration is shown in Table 3.2 below.

Table 3.2. $K_{fitting}$ consideration (Carson Ca, 2011) (Shewin Electric, 2009)

Fitting Items	Number of Items	$K_{fitting}$ Value	Total
45^0 flanged	2	0.2	0.4
90^0 bends	3	0.75	2.25
No return valves	1	1	1
Valves (fully open)	1	0.3	0.3
Total $K_{fitting}$			**3.95**

Therefore, $K = K_{pipe} + K_{fitting} = 3.95 + 42 = 45.95 \approx 46$. So, referring Equation (3.9) D_h can be calculated as (Carson Ca, 2011) (Shewin Electric, 2009),

$$D_h = 46*\frac{2.2^2}{2*9.81} = 11.34m$$

The velocity head loss can be calculated by using the following formula.

$$V_h = \frac{V^2}{2g} = \frac{2.2^2}{2*9.81} = 0.25 \tag{3.12}$$

Pump level head P_h, vertical rise head V_{Rh}, and the horizontal length of the pipe H_{pipe} are each considered to be 12m, 80m, and 8m, respectively. Consequently, by using Equation (3.2), the total system dynamic head is determined as follows:

$$T_h = f_h + D_h + H_{pipe} + P_h + V_{Rh} + V_h = (10.4 + 11.35 + 12 + 80 + 8 + 0.25)m = 122m$$

3.6. Analysis of Power Requirement

The next stage is to figure out how much power each subsystem in the proposed system needs. Calculating how much power is needed to get the water to the surface is a crucial stage. The sizes of pumps, induction motors, PV arrays, and other devices are included.

3.6.1. Pump Size

The needed hydraulic power P_h of the pump is determined as the first step of the power system analysis and is given by: (Shewin Electric, 2009)

$$P_h = \frac{q\rho g T_h}{3600*1000} \tag{3.13}$$

Consequently, the water flow rate q can be determined as follows:

$$q = \frac{Q_{fr} / day}{P_{oh}} \tag{3.14}$$

where Q_{fr} represents water flow rate and P_{oh} represents pump operation hours. The system is considered to operate for 8 hours each day (Shewin Electric, 2009).

$$q = \frac{800\, m^3/day}{8\, hr/day} = 100\, m^3/hr$$

Thus, by using Equation (3.13), the hydraulic power of the pump is determined as follows:

$$P_h = \frac{100*115,506*9.81*122}{3600*1000} = 3.84kW$$

If the efficiency of the pump is not known, the recommended value is between 65 to 70 percent (assume η=0.65).

$$P_h = \frac{q\rho gh}{\eta} = \frac{3.84}{0.65} = 5.91kW \tag{3.15}$$

Hence finally form the total dynamic head, well depth can be determined. Consider the static level is assumed to be 7m. thus, well depth is the difference between the total dynamic head and the static level which is 115m. Also, draw down is 20m and safe yield in that area is 43.2 L/s then recommended pump position is depend on the above data.

3.6.2. Induction Motor Size

Induction motor is considered for pumping the necessary water, as indicated in the previous chapters. Equation (3.16) below provides its load power (Shewin Electric, 2009). It is expected that the induction motor pump efficiency is 0.7.

$$P_m = \frac{P_h}{\eta} = \frac{5.91}{0.7} = 8.44kW \tag{3.16}$$

3.6.3. PV Panel Sizing

For comparison, the findings from (A. Tadessie,2011) (B. fola, 2020) and the NASA sunlight data are found as follows. The solar radiation from various sources is shown in Table 3.3.

Table 3.3. Solar radiation from different sources

Month	Collected (MJ/m^2)	NASA		Month	Collected (MJ/m2)	NASA
Jan	5.84	6.02		Jul	5.86	5.14
Feb	6.38	6.50		Aug	6.04	5.27
Mar	6.73	6.44		Sept	6.20	5.76
Apr	6.66	6.22		Oct	6.30	5.86
May	6.36	6.25		Nov	6.01	6.24
Jun	6.35	5.66		Dec	5.80	6.21

As can be seen from the table above, the NASA estimate of solar radiation and the data that was collected are nearly identical. The value of solar radiation obtained from NASA is used for this purpose as the input for the software and PV design. The graphical representation of solar radiation from these different sources is shown in Figure 3.4.

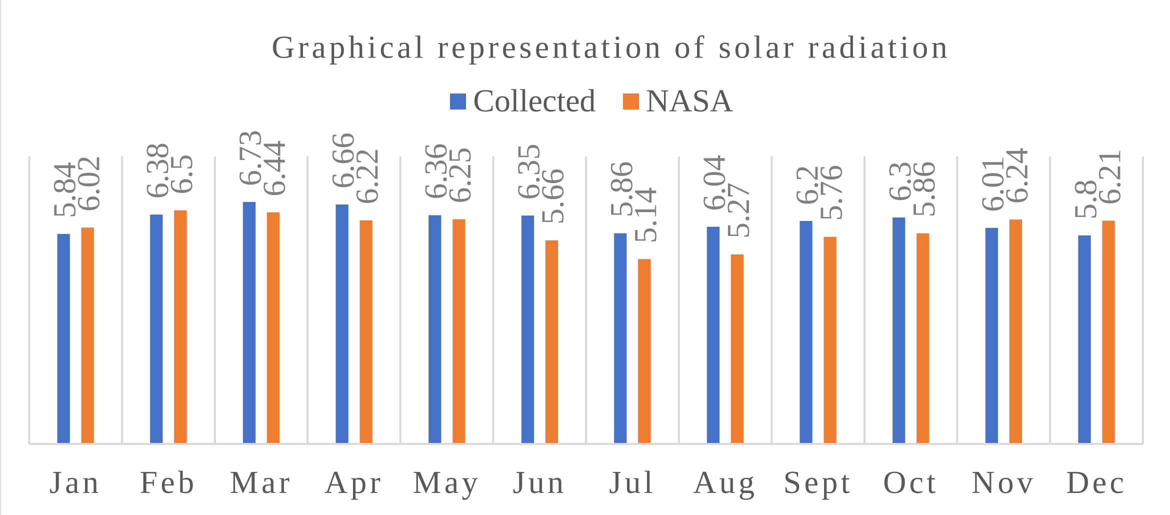

Figure 3.4. Graphical representation of solar radiation

The PV sizing needs to be well-planned in order to drive the induction motor. The system's operating time is thought to be 8 hours each day, from 8:00 AM to 4:00 PM. The daily energy consumption of E_{uses} is calculated using pump power and working hours.

$$E_{uses} = P_m \times hrs = 8440W \times 8h / day = 67,520Wh / day \tag{3.17}$$

The total daily watt-hour is divided by the mismatch factor to determine the estimated amount of PV energy required. 60 to 70% is the recommended combined efficiency. thus, 60% is chosen for the purpose of this study. Assume that the losses experienced during power conversions between the load and the PV panel are included in this total efficiency (B. fola, 2020). Therefore,

$$\text{Energy of PV } (E_{pv}) = \frac{\text{Energy Demand}}{\text{Combined Efficency}} \frac{67,520\text{Wh/day}}{0.6} = 112,533.33\text{Wh/day} \tag{3.18}$$

The size of the PV array is now determined by dividing the lowest average daily insolation by the minimal generation (G-min), which is 5140 Wh/m^2/d as shown in Figure 3.4 (S. D. Gont, 2019) J. (Uboori et al., 2016).

$$P_{PV} = \frac{E_{pv}}{G_{min}} \times 1000W/m^2 \tag{3.19}$$

where: P_{pv} is the total power of PV array in watts, E_{pv} is the total energy required from the PV array, G_{min} is the minimum solar radiation of a month that occurred in a year. Therefore, using Equation (3.19) P_{PV} power determine as:

$$P_{PV} = \frac{112,533.33\text{Wh / day}}{5140\text{Wh / m}^2\text{ / day}} \times 1000\text{W/m}^2 = 21,893.64\text{W} \quad (3.20)$$

For the sake of this study's proposed system design, the CSS-MSP-250W type of PV module is selected. The PV output power and output voltage can be used to compute the load current or PV current of the system (S. D. Gont, 2019) (J. Uboori et al., 2016).

$$I_{pv} = \frac{P_{pv}}{PV_{\text{output voltage}}} = \frac{21,893.64\text{W}}{220\text{V}} = 99.52\text{A} \quad (3.21)$$

The number of PV modules in parallel (N_p) is determined using Equation (3.22):

$$N_p = \frac{I_{PV}}{PV_{\text{Short circuit current}}} = \frac{99.52\text{A}}{7.79\text{A}} = 12.78 \approx 13 \text{ modules} \quad (3.22)$$

Equation (3.23) can also be used to get the number of series modules NS from the PV module's output voltage and open circuit voltage.

$$N_s = \frac{V_{PV}}{PV_{\text{open circuit voltage}}} = \frac{220\text{v}}{30.8\text{v}} = 7.14 \approx 8 \text{ modules} \quad (3.23)$$

Equation (3.24) is then used to calculate the total number of modules in the PV array for the CSS-MSP-250W PV type, as illustrated below:

$$N_T = N_p \times N_s = 13 \times 8 = 104 \text{ modules} \quad (3.24)$$

Consequently, 104 modules are needed in total to produce the desired design.

3.6.4. Photovoltaic Model

A PV module is made up of a variety of numerous photovoltaic cells that are coupled in series and parallel in order to boost the PV current and deliver a high output voltage, respectively. The load current, solar irradiation, and temperature all affect the DC voltage that the PV modules produce (Emmanuel Kwaku Anto et al., 2016) (K. I. Mirza Mursalin Iqbal, 2017) (A. Omar et al., 2014). The PV model with a single diode circuit, series resistance, and parallel is the one that is most frequently used in PV modelling to forecast how much energy will be produced by solar cells.

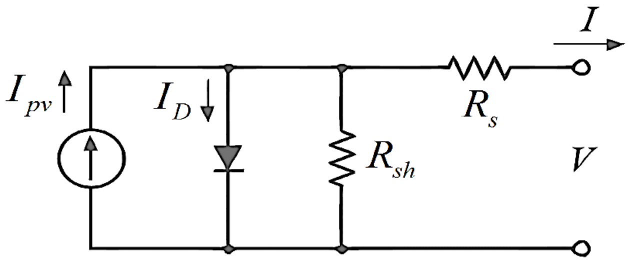

Figure 3.5. Equivalent circuit of PV model using single diode.

The parameters of the chosen PV array (CSS-MSP-250W), which are provided in Table 3.5, as described in the preceding section and are crucial for modelling the PV array (Online5, 2023). The following equations (Emmanuel Kwaku Anto et al., 2016) (A. Omar et al., 2014) can be used to explain the mathematical model of a PV cell. Using Kirchhoff's current law, the equivalent circuit diagram shown in Figure 3.5 is generated.

$$I = I_{pv} - I_d - \frac{V_d}{R_{sh}} \tag{3.25}$$

A diode current can be represented as;

$$I_d = I_o \ [\exp (q (\frac{V_{pv} + I_{pv} R_s}{a \times K \times T}) - 1] \tag{3.26}$$

The shunt current is represented as;

$$I_{sh} = (\frac{V_{pv} + I_{pv} R_s}{R_{sh}}) \tag{3.27}$$

Where: an is the diode ideality factor, I_{scn} is the short-circuit current at the nominal condition, K is the Boltzmann constant (1.38×10^{-23} JK^{-1}), N_S is the number of cells connected in series, N_S is the number of cells connected in parallel, q is the electronic charge (1.602×10^{-19}), R_p is the shunt resistance (Ω), and R_s is the series resistance (Ω).

The equivalent circuit current is calculated using the three equations above, as indicated in Equation (3.28).

$$I = I_{pv} - I_o \ [\exp(q(\frac{V_{pv} + I_{pv} R_s}{a \times K \times T}) - 1)] - (\frac{V_{pv} + I_{pv} R_s}{R_p}) \tag{3.28}$$

From Equation (3.25), also light generated current I_{pv}

$$I_{pv} = \frac{G}{G_n} (I_{pvn} + K_i \left(T - T_{ref} \right) \tag{3.29}$$

Also, the output current I_o are determined from Equation (3.25) as:

$$I_o = \frac{I_{sc} + K_i \Delta T}{\left(\exp \frac{V_{oc} + K_v \Delta T}{V_t \times a} \right) - 1} \tag{3.28}$$

The parallel and series connections between the modules make up the PV module model. Equation (3.25) is therefore changed to the following equation:

$$I = ((N_p I_{pv} - N_p I_o)\ [N_p I_o)\ [\exp[(V + IR_s \times (N_s) / (N_p)) / (aV_t N_s)] - 1])) \tag{3.29}$$

where: V_d is the voltage across the diode; V_{ocn} is the open circuit current at the nominal condition; V_{tn} is the voltage thermal at the nominal condition; T is the module operating temperature in Kelvin; and ΔT is the deviation from the nominal temperature in Kelvin; I_d is the diode saturation current; I_{PV} is the light generated current of the photovoltaic cell; G is the actual irradiance in W/m^2; and G_n is the irradiance at the nominal condition.

Table 3.4. Electrical characteristics for photovoltaic array specification (Online5, 2023).

Parameters	Description	Value
-	Cell efficiency	17.24%
I_{mp}	Current at P_{max}	7.79A
I_{sc}	Current temperature coefficient α	0.02%/ ^{0}C
V_{oc}	Open-circuit voltage	37.4V
R_P	Parallel resistance of PV model	37.404Ω
P_{max}	Peak Power	250W
p_{max}	Power temperature coefficient γ	-0.42%/ ^{0}C
-	Series fuse rating	15A
R_S	Series resistance of PV model	0.23219 Ω
I_{sc}	Short-circuit current	8.49A
V_{mp}	The voltage at P_{max}	30.8V
V_{oc}	Voltage temperature coefficient β	- 0.31%/ ^{0}C

The following equations (B. Alsayid, 2012) (Y. Zhang, 2017) indicate an investigation into the mathematical analysis of the chosen PV model parameters based on the data presented in Table 3.4. In consideration of the open circuit voltage, maximum peak voltage of the modules, and maximum peak current, the short circuit or series resistor is determined.

$$R_s = \frac{V_{oc} - V_{mp}}{I_{mp}} = \frac{37.4 - 30.8}{7.79} = 0.847\Omega \tag{3.30}$$

Also, the shunt resistance is determined as follows in Equation (3.31):

$$R_{sh} = \frac{I_{sc}R_s - V_{oc}}{I_{mp} - I_{sc}} = \frac{(8.49 \times 0.847) - 37.4}{7.79 - 8.49} = 43.15\Omega \tag{3.31}$$

A PV array is modelled using MATLAB/Simulink and is based on the mathematical equation of the solar system. The relevant parameters for PV array modelling, including I_{sc}, G, N_s, N_p, K_t, T_{ref}, and V_{oc}, are provided in Table 3.5 and obtained from the description of the PV module selected for the standalone system. Different irradiances at constant temperature are used to model the PV array. The series and parallel PV modules, which were determined from the analysis in the previous section, are used to determine the actual output voltage and current.

$$V_{PV} = V_{mpp\ module} \times N_s = 30.8 \times 8 = 246.4v \tag{3.32}$$

$$I_{PV} = I_{mpp\ module} \times N_p = 7.79 \times 13 = 101.27A \tag{3.33}$$

The entirely Simulink design of the PV model is constructed as illustrated in Figure 3.6 based on the above-mentioned mathematical modelling. In Appendix A, each subsystem model is presented.

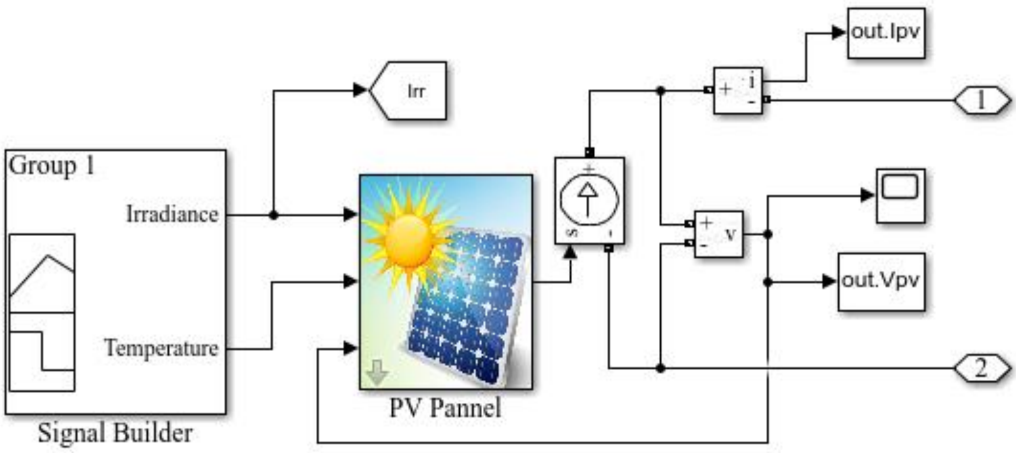

Figure 3.6. Simulink diagram of PV module design

The relationship between the current and power of the PV module can be determined with a variety of temperatures and irradiances. The I-V and P-V characteristic curves are presented with G values of 400W/m^2, 800W/m^2, and 1000W/m^2 with the temperature fixed at 25°C.

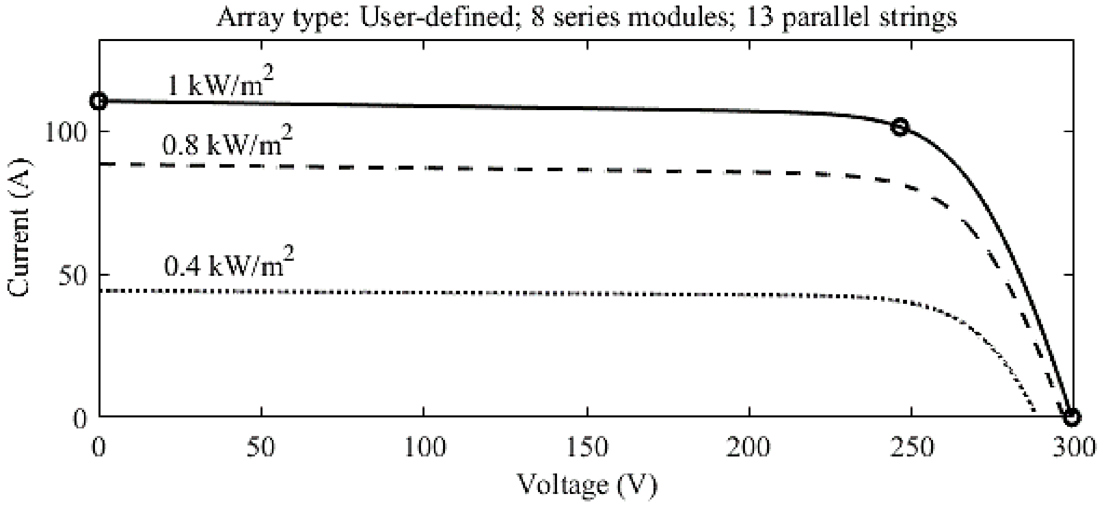

Figure 3.7. I-V characteristic curve of PV panel at different irradiances

The nonlinear curve is dependent on both the temperature and solar irradiation. As the irradiation increases, the maximum power point likewise increases and the current increases more than the voltage, as seen in Figures 3.7 and 3.8. The short circuit current is greatly influenced by how a PV array responds to various levels of solar radiation and a constant temperature. Nevertheless, it little affects the open-circuit voltage. Consequently, the PV array produces more energy when solar radiation increases.

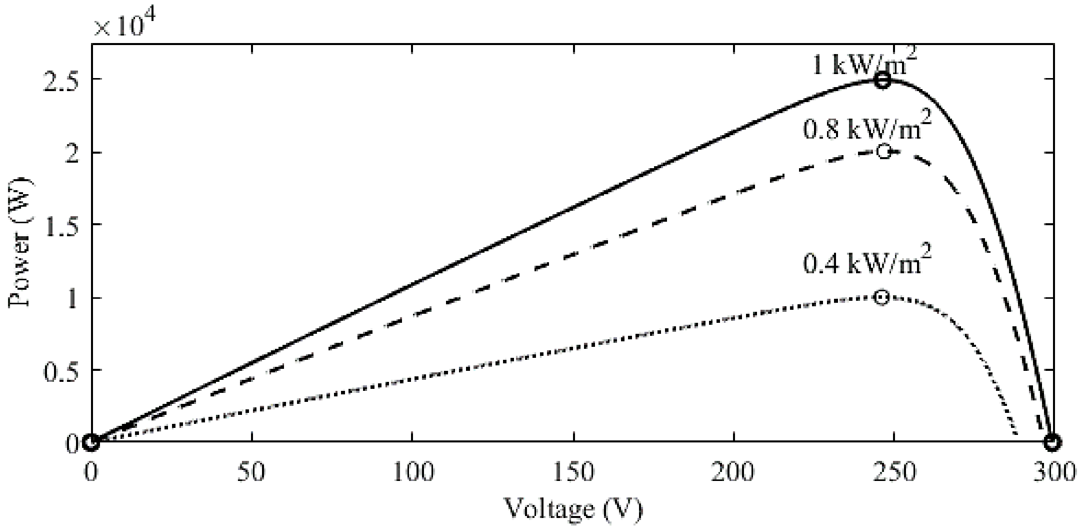

Figure 3.8. P-V characteristic curve of PV panel at different irradiances

3.6.5. Modeling of DC-DC Boost Converter

DC-to-DC converters can be divided into three categories: boost, buck, and buck-boost (Emmanuel Kwaku Anto et al., 2016) (J. Grant, 2018). The boost converter is taken to be considered for this analysis with a reference DC link voltage of 220 volts and an output voltage of 400 volts at a switching frequency of 10 kHz. The circuit is presented in Figure 3.9 and its primary parameters, including inductance, capacitance, diode, and resistor, were designed. The PV array is shielded from the negative current by the diode. Additionally, the capacitor is placed here to reduce the high-frequency harmonics, and it switches in the manner described below.

- The voltage across the inductor is $V_L = V_{in}$ when the switch shown above is closed. The inductor's current increases linearly. The diode is reverse-biased by voltage, which prevents current from flowing through it.
- When the switch is opened, the voltage across the inductor is $V_L = V_{in} - V_o$ (neglecting the drop across the diode), and the diode is forward biased. In the ON condition, the inductor current increased; now, it drops.

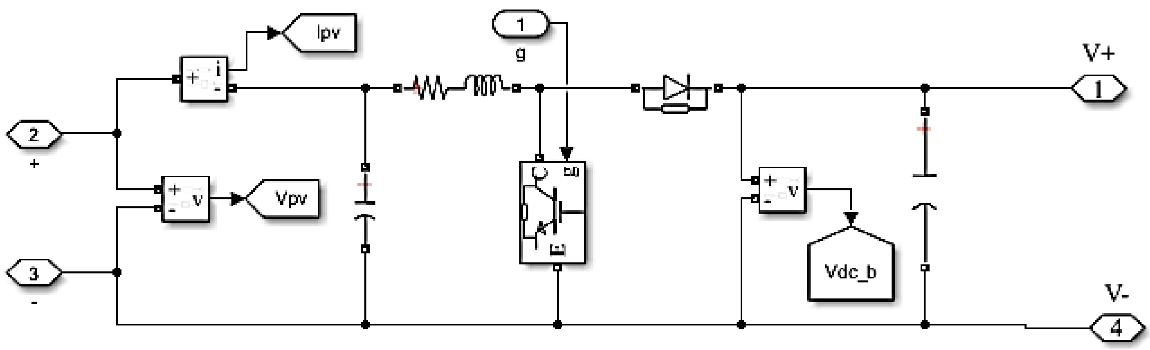

Figure 3.9. Modeling of the boost converter

As a result, the induction motor's load is 8.44 kW, and the output voltage V_o is 400 V in the design of the DC-DC boost converter. Additionally, the output voltage or input voltage V_{in} of the boost converter is 246.6V according to the PV analysis in Equation (3.32).

As a result, Equation (3.34) illustrates the boost converter's output and input voltage relationship.

$$V_o = \frac{V_s}{1 - D} \tag{3.34}$$

Rearranging Equation (3.34), the maximum duty ratio for extracting 400v output voltage is:

$$D = 1 - \frac{V_{in}}{V_o} = 1 - \frac{246.4\text{v}}{400\text{v}} = 0.384 \tag{3.35}$$

The output power must be known in order to calculate the DC load; hence the following formula is used to calculate the DC load resistance:

$$R = \frac{V_{out}^2}{P} = \frac{400^2 v}{8440 w} = 18.96\Omega \tag{3.36}$$

Inductor Calculation: The filter inductor value and its peak current are determined based on the specified maximum inductor current ripple (M. B. Kumar, 2018).

$$L \geq \frac{D \times (1 - D)^2 \times R}{2 f_s} \tag{3.37}$$

$$L_{min} = \frac{0.384 \times (1 - 0.384)^2 \times 18.96}{2 \times 20000} = 0.112 mH$$

Capacitor Calculation: The function of the capacitor is to filter the inductor current ripple and passing a stable output voltage (M. B. Kumar, 2018). It also has to ensure that load steps at the output supported before the regulator is able to react.

$$C = \frac{D}{r \times f_s \times R} \tag{3.38}$$

where: r is the ripple factor of the boost converter output voltage and it is considered as a maximum of 4% which means that the ripple voltage will be 16v.

$$C = \frac{0.384}{0.04 \times 20000 Hz \times 18.96\Omega} = 25.32 \mu F$$

where: D is duty cycle (%), f_s is switching frequency (Hz), L is inductance (H), and R is resistance (Ω) of the load.

3.6.6. Inverter Sizing

The inverter must be sized so that it can manage the maximum expected power of the AC load. Therefore, it should be considered 25-30% greater than the total AC-rated power (S. D. Gon, 2018). The inverter's rated power changes to 8440W + (0.26×8440W) = 10,634.4W. As a result, CSI-10KTL1P-GI-FL inverter, which has 11.5kW×2 inverters and can handle continuous power ratings, was chosen as the inverter for the proposed PV system.

3.6.6.1. Analysis of DC Link Capacitor

This method of determining the DC link capacitor's minimum capacity is dependent on the estimation of the maximum input power step and the definition of the maximum permitted voltage deviation. A common restriction is a 10% DC link voltage fluctuation at any step-on and step-off load response. The solar panel power at its maximum power point (MPP) is equal to the anticipated maximum input power step. The DC/DC converter's control delay is represented by the time constant Tr, and a value of, for example, five to ten modulation periods is a reasonable choice (H. Raffel, 2003). Starting with the energy ΔW, which is calculated as:

$$\Delta W = \int_0^{T_r} \Delta P_{max}.dt = \Delta P_{max}.T_r \tag{3.39}$$

The capacitor's stored energy can be expressed as follows:

$$W = \frac{1}{2} C_d V_d^2 \tag{3.40}$$

Additionally, depending on the DC link voltage V_d, the DC link voltage deviation ΔV_d, and the capacity C_d, the fluctuation of the capacitor's stored energy can be approximated as follows:

$$\Delta W = \frac{1}{2} C_d (V_d + \Delta V_d)^2 - \frac{1}{2} C_d V_d^2 \tag{3.41}$$

The minimal capacity $C_{d,min}$ is expressed as the combination of Equations (3.39) and (3.41):

$$C_{d,min} \geq \frac{T_r.\Delta P_{max}}{(V_d \Delta V_d + \frac{1}{2} \Delta V_d^2)} \tag{3.42}$$

In (H. Raffel, 2003), the transferred energy ΔW by the capacitor bank is approximated as follows, providing another way to understand the minimal DC link capacity:

$$\Delta W = \frac{T_r.\Delta P_{max}}{2} \tag{3.43}$$

The voltage deviation is given by:

$$\Delta V_d = \frac{\Delta W}{C_d V_d} \tag{3.44}$$

This results in the following equation for the minimum capacity, $C_{d,min}$:

$$C_{d,min} \geq \frac{T_r.\Delta P_{max}}{2.V_d \Delta V_d} \quad (3.45)$$

Equations (3.42) and (3.45) can be compared, and it can be observed that the increase in gives approximately double the values of the minimal capacity (H. Raffel, 2003) by assuming a DC link voltage deviation V_d of the commonly used 10%.

3.6.6.2. Filter Design of Inverter

High power density and a reduction in system weight, size, and cost are market requirements in the design of today's power electronic converters. Electromagnetic Interference (EMI) is a significant issue associated with contemporary motor drives. A filter is specifically needed for an inverter to supply power at a fixed frequency. Power converters and output filters are necessary to reduce EMI and provide dependable operation (Mishra, P et al, 2020).

Moreover, the LC filter type smooths inverter output current and voltage waveforms, decrease vibrations and common mode noise from the motor, and radiated noise from the wires. It has two components, an inductor on the inverter side and a filter capacitor. The inverter's switching frequency is therefore set at 10 KHz. Applying Equation (3.46) will help to determine the inductance value (Mishra, P et al, 2020).

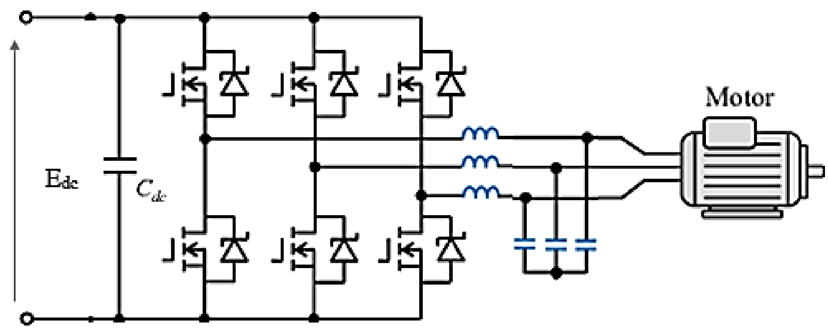

Figure 3.10. Inverter and LC filter with induction motor configuration

To determine the values of inductance (L) and capacitance (C) for a low-pass filter that achieves a current THDc of 5% in a three-phase inverter with an output current of 36 A and a voltage of 400 V, the following analysis is followed the steps outlined below:

- The fundamental current (I_f) is calculated as: output current / √3 = 36 A / √3 = 20.78A
- Determine the maximum allowable harmonic current (Ih_max) based on the desired THDc value: Ih_max = (THDc (%) / 100) x I_f = (5%/100) x 20.78A = 1.039A

- The harmonic order (n) for the switching frequency of 10kHz and fundamental frequency of 50Hz is 200, which is useful for the design of low-pass filter.
- Then the impedance (Zn) is calculated for the design of low-pass filter at the harmonic order (n): Zn = Output Voltage / Ih_max = 400v/1.039A = 384.98 Ω.
- Determine the angular frequency (ω) based on the fundamental frequency (f): ω = 2πf = 314rad/sec. Then inductance (L) is calculated as:

$$L = Zn / (\omega \times n) = 384.98\ \Omega / (314 \times 200) = 6.13\text{mH} \tag{3.46}$$

The other element considered to be analyzed in the filter design is capacitance value and can be calculated by applying the following Equation (3.47) (Mishra, P et al, 2020).

$$C = 1 / (Zn \times \omega \times n) = 1/(384.98\ \Omega \times 314 \times 200) = 0.042\mu\text{F} \tag{3.47}$$

The following Table 3.5 depicts the specifications of the induction motor used for this study. It is a three-phase motor and there is no need of speed control for the water pumping. This motor can operate at a rated speed if the input voltage is properly maintained.

Table 3.5. Induction motor specifications.

Parameters	Value [Unit]
Stator phase inductance	0.0001 [H]
Stator winding resistance	9.6 [Ω]
Control input rated voltage	400 [V]
Moment of inertia the rotor	0.0343[kg·m^2]
Number of poles	2
Rated motor power	10 [kW]
Rated speed	1500 [rpm]
Friction factor	0.000503 [N·s/m]

3.7. Economic Analysis

This study analyses the net present cost in order to calculate the cost of standalone PV analysis since it is crucial for evaluating the economic behavior of renewable energy systems. All system component expenses, including capital costs, replacement costs, operating costs, and maintenance costs, are covered.

All system components, including the PV panel, converter, inverter, and installation, are included in the system's initial capital cost. The second consideration is the cost of operation and maintenance (O&M), which includes annual periodic costs, site management, and routine maintenance. The last one is the replacement cost, which is necessary for ongoing operation because, depending on their nature and operating environment, some system components must be replaced on a regular basis (S. D. Gont, 2019) (T. El Shenawy et al, 2017). Cost estimation of the standalone PV system is discussed as following suggestions.

- The system has a high capital cost (initial cost).
- The price of maintenance is relatively low.
- Fuel costs are nonexistent.
- The price of replacement parts is low.

$$\text{Replacement cost} = A_1\left(\frac{1+i}{1+d}\right)^n \tag{3.48}$$

where: A_1 is the initial cost of the inverter and converter, n is a lifetime in years, i is a discount rate at 4% or 0.04 and discount rate (d) of 8%,

Table 3.6. Cost of standalone PV component**s**

No.	Component	Capital cost	Replacement cost	O&M cost/year	Lifetime (years)
1	PV panel	$2/Watt	$47,840	$3510	20
2	Converter	$3907/unit	$2639.42	$100	10
3	Inverter	$5348/unit	$5348	$100	20

- PV panel initial cost = $2/W × 104 × 230W = $47,840
- Inverter cost = $5348
- Replacement cost of converter $= 3907\left(\frac{1+0.04}{1+0.08}\right)^{10}$ = $2678.79
- Total replacement cost = $2,678.79+$47,840+$5,348 = $55,866.79
- Total O and M cost = $3510 + $100 +$100 = $3710
- Installation cost = 0.1× $47,840 = $4,784 (1% of PV cost is taken for installation).

O&M costs are estimated to be 2% of the $965.8 total initial PV cost. By considering discount rates and inflation, the annual O&M costs of the PV panel may be computed based on the initial capital cost as follows:

$$O\,\&\,M = 2\%PV \times \frac{1+i}{1+d} \times \left[\frac{1 - (\frac{1+i}{1+d})^{n}}{1 - (\frac{1+i}{1+d})} \right] \tag{3.18}$$

$$O\,\text{and}\,M = 0.02 \times \$47,840 \times \frac{1+0.04}{1+0.08} \times \left[\frac{1 - (\frac{1+0.04}{1+0.08})^{25}}{1 - (\frac{1+0.04}{1+0.08})} \right] = \$15,193.26$$

The total cost of the PV system's components, total replacements, inverter, installation, operation, and maintenance expenses were added to get the net present cost of the PV system.

$$\text{NPC} = PV_c + Inv_c + C_c + Inst_c + O\,\&\,M + \text{Total}\,rep_c \tag{3.49}$$

NPC = $47,840 + $5,348 + $3,907 + $15,193.26 + $55,866.79 = $128,155.05

Additionally, it's crucial to determine a system's overall annualized cost [$/year] on an annual basis. The PV's annualized total cost [$/year] in terms of the current exchange rate is assessed in (T. El Shenawy et al, 2017) (Y. S. Mohammed Kharrich et al, 2017). The following formula can be used to compute the total annualized cost [$/year]:

Total annualized cost [$/year];

$$C_{ann,tot} = NPC \times CRF \tag{3.50}$$

where CRF indicates the capital recovery factor and Equation (3.51) depicts its equation;

$$\text{CRF} = \left[\frac{i \times (i+1)^{n}}{(1+i)^{n} - 1} \right] \tag{3.51}$$

$$\text{CRF} = \left[\frac{0.04 \times (0.04+1)^{25}}{(1+0.04)^{25} - 1} \right] = 0.064$$

Thus, by applying Equation (3.50) the total annual cost is found as:

$$C_{ann,tot} = \$128{,}155.05 \times 0.064 = \$8201.9232$$

Equation (3.51) illustrates how the total annualized cost and the annual energy produced by the photovoltaic system may be used to determine the cost of energy (COE) (T. El Shenawy et al, 2017).

$$\mathrm{COE} = \frac{\mathrm{C_{ann,tot}}}{365 \times \mathrm{E_{load}}} \tag{3.22}$$

$$\mathrm{COE} = \frac{8201.9232\$}{365 \times 112.533\mathrm{kWh/yr}} = \$0.20/\mathrm{kWh}$$

The objective of the economic analysis is to improve the system's reliability and efficiency, as was described in this section. Additionally, the standalone system needs to be economical. The NPC is seen as a system objective function. In most cases, the net present cost is an essential aspect of a standalone PV system's design.

CHAPTER FOUR

FUZZY BASED P&O MPPT CONTROLLER DESIGN

4.1. Block Diagram of the Proposed Controller

The method used for this thesis entails a variety of tasks that are carried out in order to result in completion. The PV array, MPPT, DC-DC boost converter, induction motor, and pump load constitute the main component of the proposed system. PV arrays are employed in this thesis to produce DC power from solar energy, and fuzzy-based P&O MPPT is added to it to track the maximum power. The PV array's output voltage is then scaled up using a DC transformer also known as a boost converter.

The output of the boost converter is controlled using a fuzzy-P&O MPPT controller to obtain a stable and smooth response. The output of the buck converter is then converted to AC power with the help of an inverter, and signal generator PWM techniques are used to trigger the power semiconductor device. Figure 4.1 depicts the proposed system's layout.

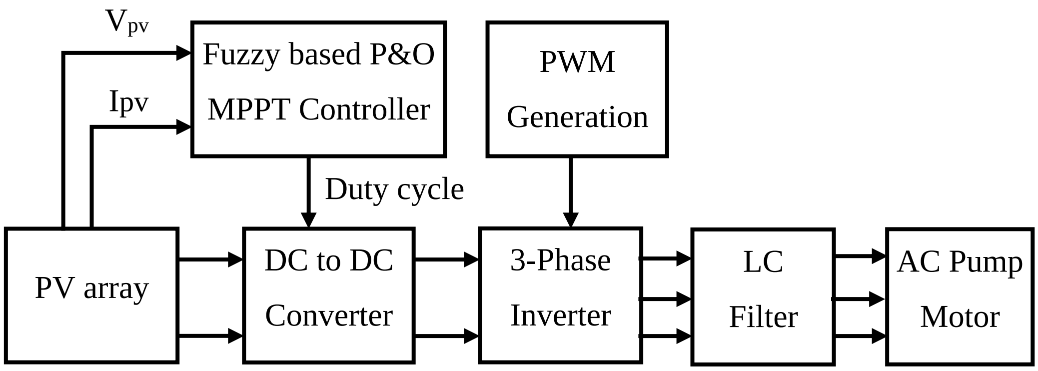

Figure 4.1. The layout of proposed system

To get the maximum power possible out of a PV module with variable irradiance and constant temperature, an MPPT is used. The maximum power point (MPP) of a PV module is the point at which it generates the maximum energy. The PV module may not operate at the MPP when temperature and irradiance change (Abdullah M. Noman, et al., 2012).

The temperature and solar cell irradiance affect the output power induced in the PV module. Therefore, monitoring the MPP of the PV array is crucial for improving the efficiency of this renewable energy source (E. Matagne et al, 2012). The PV module has a special operating point where it can supply the load with the maximum energy. Figure 4.2 illustrates the MPP, which is a nonlinear change with cell temperature and sun irradiation. In the case of an IV curve or a PV curve, the MPP is the "knee" of the curve (E. Matagne et al, 2012).

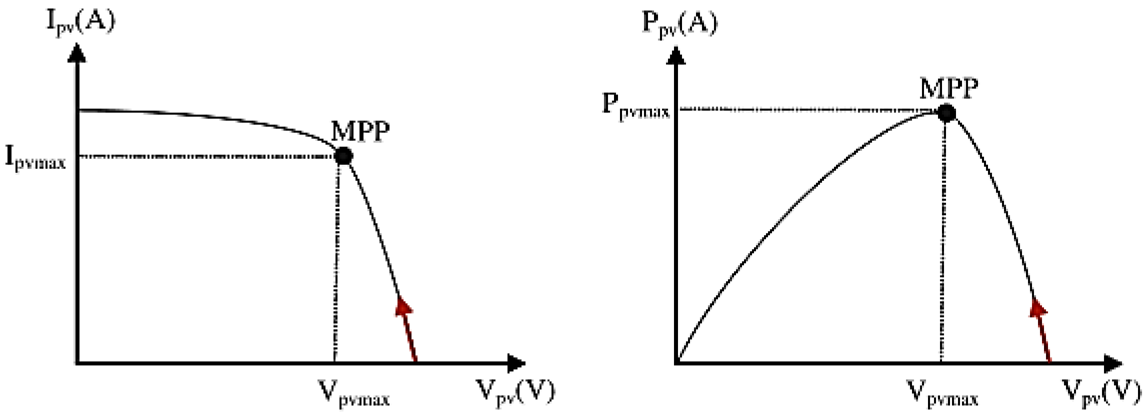

Figure 4.2. Maximum power points of IV and PV curves.

The power obtained at MPP increases with a higher solar irradiation at constant temperature, and its values vary according on the environmental factors.

4.2. Perturb and Observe (P&O) MPPT Control Algorithm

Due to its simple implementation and better conversion efficiency, the P&O algorithm is the MPPT method that solar PV panels most frequently use (Hussein Selman, 2016). It is a hill-climbing algorithm; as voltage rises, generated power rises along with it until the MPP is attained. When MPP is reached, as illustrated in Figure 4.3, the generated power drops as the voltage rises. However, this method is more effective when there is less of an environmental change. One global maximum and numerous local maxima are produced when the environment changes in the PV characteristics.

The P&O algorithm's output power mainly follows local maxima. Since the seasons in Ethiopia are unpredictable, it is impossible to produce the same amount of output power all year long (E. Matagne et al, 2012) (Dilovan Haji, et al., 2018). The generated power and other factors, such the output voltage of the PV, are susceptible to larger oscillations even though it is good in a certain range of environmental change. Also, reaching stable state will take longer.

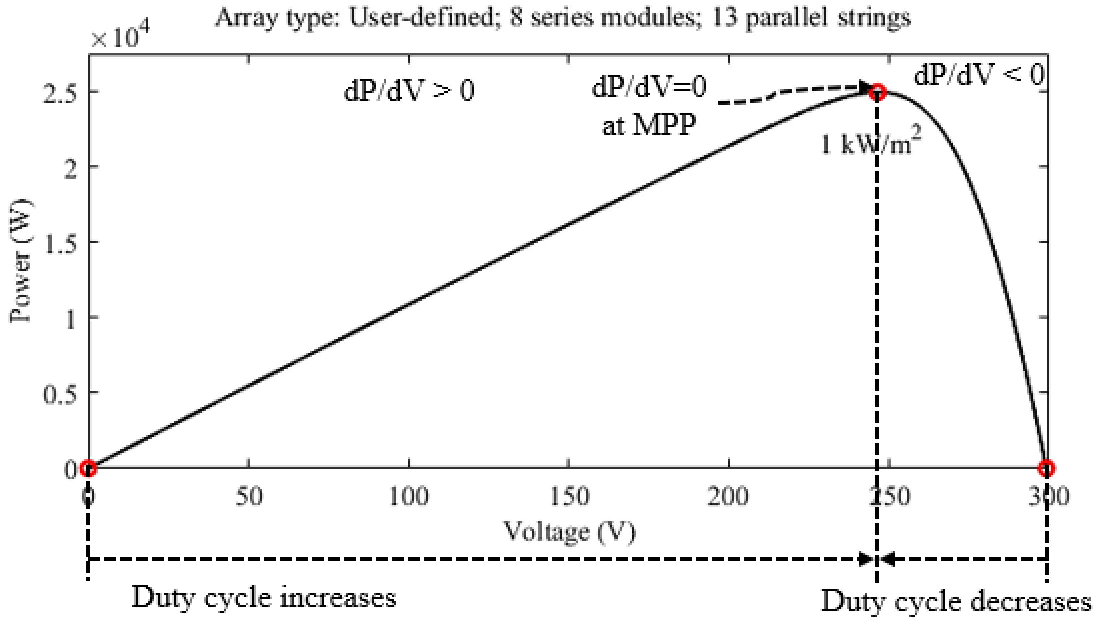

Figure 4.3. MPPT tracking, by changing the duty cycle.

A flowchart of the algorithm implemented in the Simulink model for the P&O is presented in Figure 4.4, while the Figure 4.3 shows how the duty cycle changes regarding the voltage variation and power generated by the solar panel.

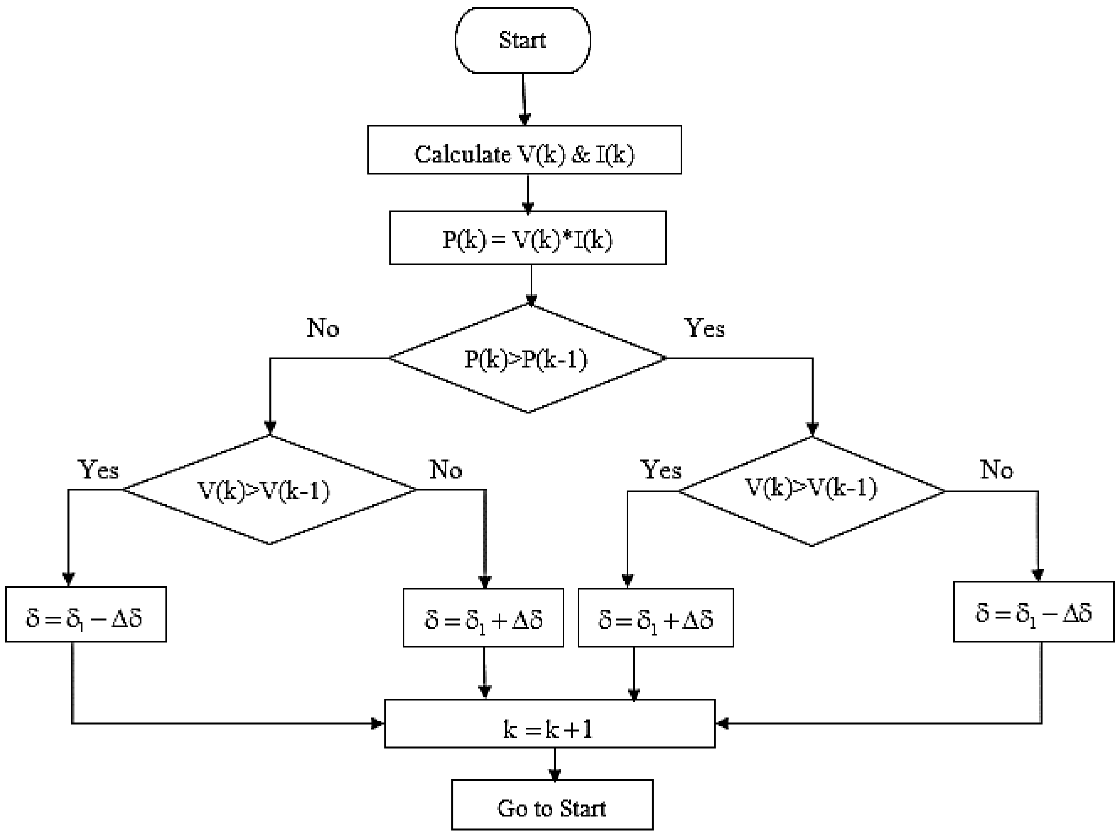

Figure 4.4. Flowchart of the P&O algorithm, implemented in the controller model.

The P&O algorithm compares and assesses the PV voltage and generated power between iterations, and then adjusts the duty cycle in accordance, as shown in Figures 4.3 and 4.4. The duty cycle is left unchanged if the generated power is constant between iteration; otherwise, the PV voltage is compared, and the duty cycle is adjusted accordingly until it hits MPP.

Consequently, the best ways to track the global maximum are via AI-enhanced P&O algorithms. In the sections that follow, a more thorough explanation of both the conventional P&O strategy and the fuzzy enhanced approach is provided.

4.3. Fuzzy Based P&O MPPT Controller

Fuzzy logic has recently been introduced for the MPPT of a PV system, as it is being utilized to improve the efficiency of conventional MPPT techniques like the P&O and Incremental Conductance algorithms. Traditional MPPT algorithms that have been modified are more reliable and have the benefit of not needing precise model information for their design process (E. Matagne et al, 2012) (Dilovan Haji, et al., 2018). The FLC's primary steps can be divided into three categories: defuzzification, inference rules, and fuzzification. Figure 4.5 shows these phases as well as the controller's overall architecture.

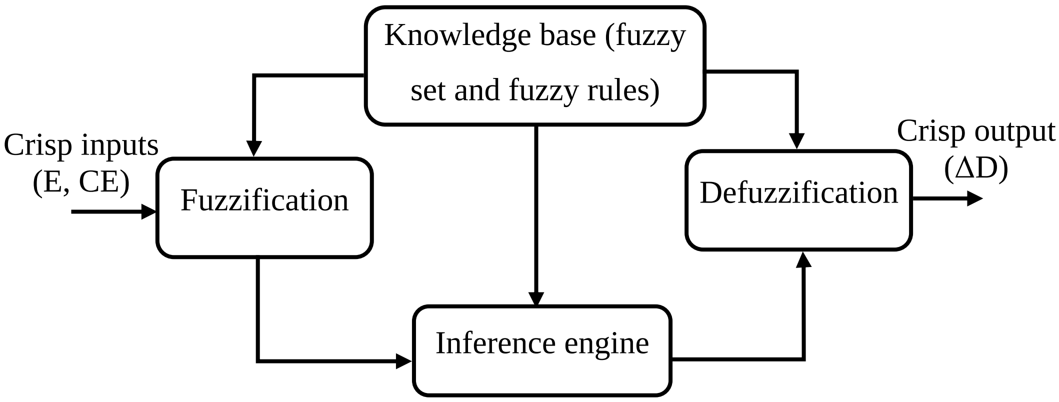

Figure 4.5. Typical architecture of a Fuzzy Logic Controller (FLC).

In the initial step, referred known as fuzzification, crisp inputs are combined with stored membership functions that are assigned to each input to create fuzzy inputs. After completing this phase, the controller needs to produce its input values by comparing real-time inputs with stored membership function data. Figure 4.6 also depicts a Simulink model of the developed fuzzy logic controller, which has two inputs and one output.

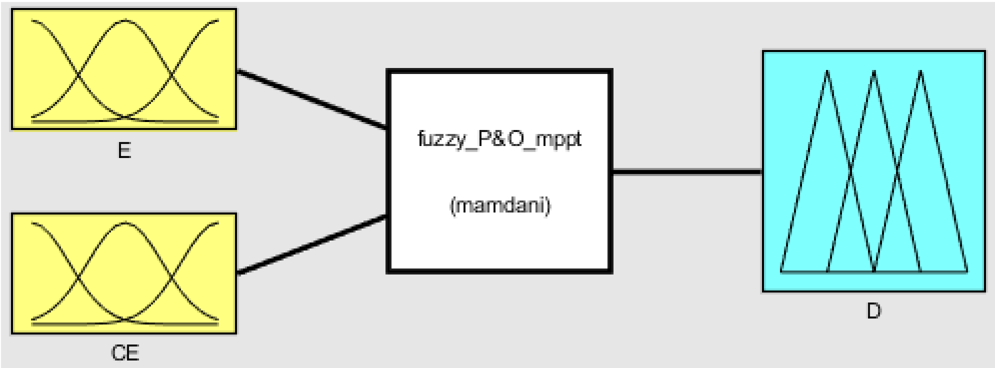

Figure 4.6. Fuzzy logic Simulink model

The error (E) and change of error (CE) at an instant k, which are given by Equations (4.1) and (4.2), are used as the inputs for the proposed FLC.

$$E(k) = \frac{P(k) - P(k-1)}{V(k) - V(k-1)} \tag{4.1}$$

$$CE = E(k) - E(k-1) \tag{4.2}$$

Equations (4.3) and (4.4) should be used to compute the change in the output voltage and output power of the PV panel, respectively, in order to derive E.

$$\Delta V = V(k) - V(k-1) \tag{4.3}$$

$$\Delta P = P(k) - P(k-1) \tag{4.4}$$

where, Vpv(k) and Ppv(k), are the measured output voltage and the power of the PV panel at the sample time n. At the first step simulation, both the output voltage and the power have an arbitrary value to initialize the system.

According to the explanation in Section 4.1, the change in output voltage and output power is utilized to determine whether the duty cycle should be increased, decreased, or held constant. The FLC allows a variable step size value to be set, which will be determined by the membership functions and the inference rules, to address this limitation and improve system performance both in steady state conditions and in the response to changing environmental circumstances.

Fuzzy logic controllers are used in the modified P&O MPPT algorithm, as indicated in the flow chart. Based on the PV voltage and current, Figure 4.7 P&O is utilized to generate the error and change of errors. The duty cycle ratio is then calculated and optimized using the fuzzy logic controller.

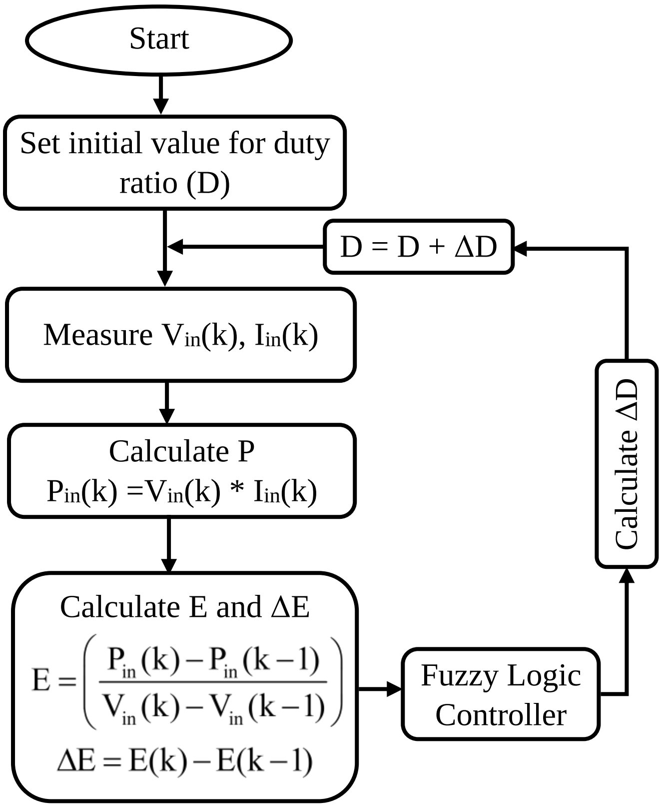

Figure 4.7. Flow chart of enhanced P&O algorithm using fuzzy logic controller

Membership function: For both input and output variables in this thesis, a triangular-based membership function is used. For certain input and output, Figure 4.8 shows a triangle membership function (E. Matagne et al, 2012) (Dilovan Haji, et al., 2018).

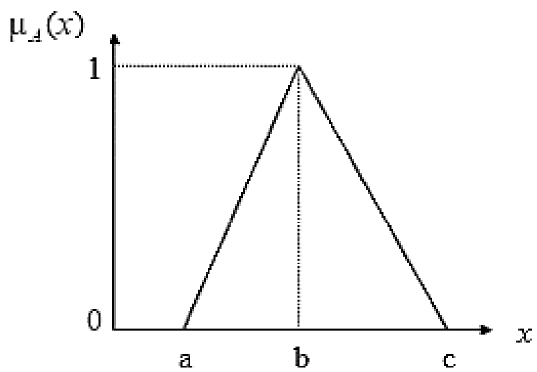

Figure 4.8. Triangular memebrship function structure

where x is the real value (Crisp Value) from the private variable fuzzy universe of discourse, and a, b, and c are the coordinates for the capital triangle.

The value of the degree of membership of x is represented by the function's output, which ranges between 0 and 1. The components between a and b gradually increase their membership degree closer to the element of b, while the elements between b and c gradually decrease their membership degree closer to the element of c. The evaluation of the specified membership function in Figure 4.8 is described by Equation (4.5) (E. Matagne et al, 2012) (Dilovan Haji, et al., 2018).

$$\mu_A(x) = \begin{Bmatrix} 0 & if\, x \le a \\ \frac{x-a}{b-a} & if\, a \le x \le b \\ \frac{c-x}{c-b} & if\, b \le x \le c \\ 0 & if\, x \ge c \end{Bmatrix} \tag{4.5}$$

Equation (4.6) can be used to determine the final step of any fuzzy model's triangle membership function.

$$trimf(x; a, b, c) = max(min(\frac{x-a}{b-a}, \frac{c-x}{c-b}), 0) \tag{4.6}$$

Five fuzzy subsets are used to assign the membership function values to the linguistic variables: NB (Negative Big), NS (Negative Small), ZE (Zero), PS (Positive Small), and PB (Positive Big). Figures 4.9 to 4.11 illustrate the membership function's shape and the fuzzy subsets' partition, which can be modified to appropriate the system.

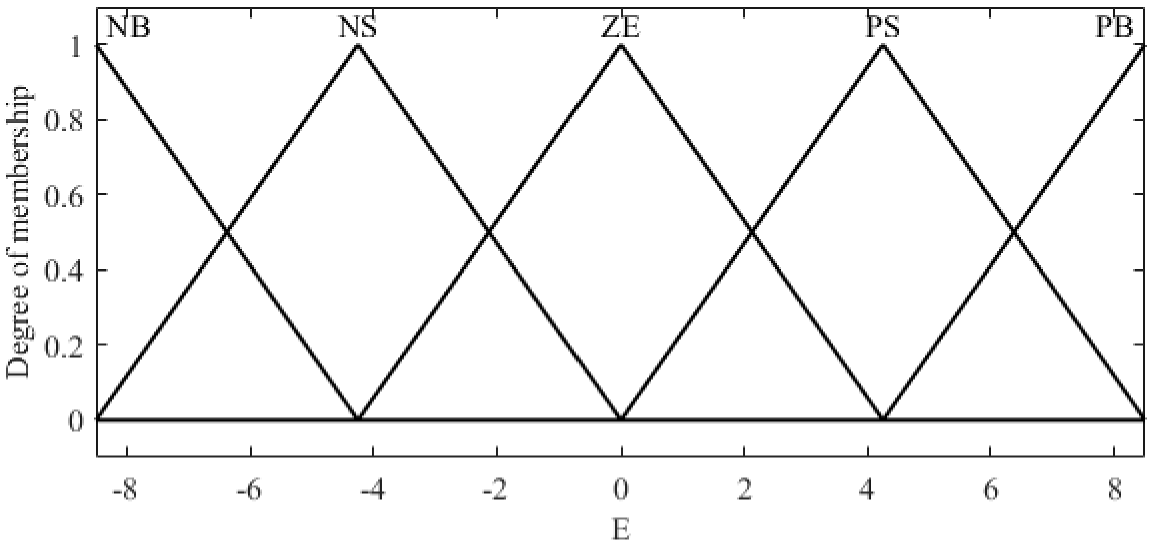

Figure 4.9. Input variable error (E) membership function

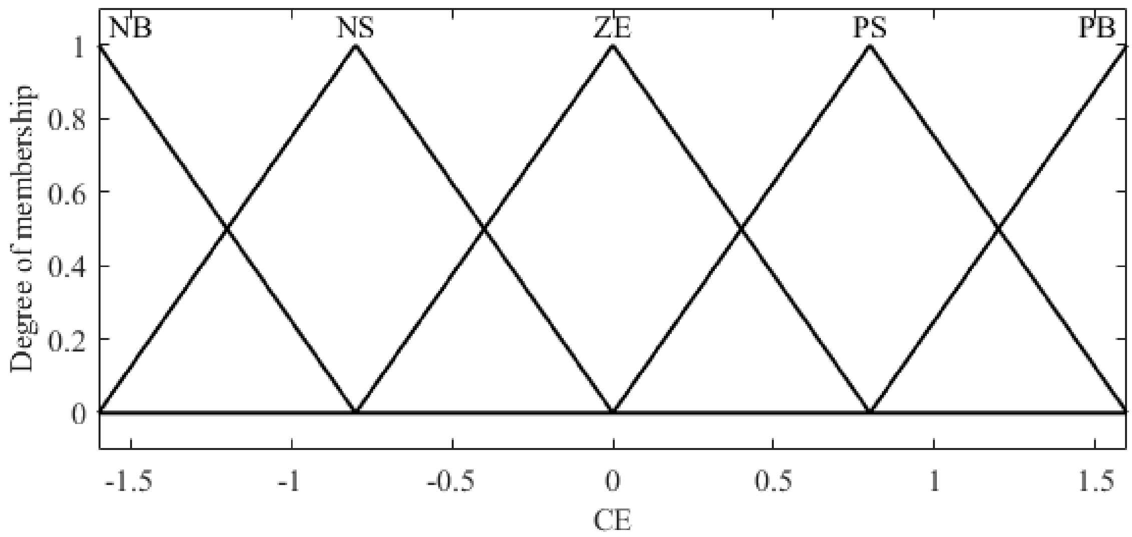

Figure 4.10. Input variable change of error (CE) membership function

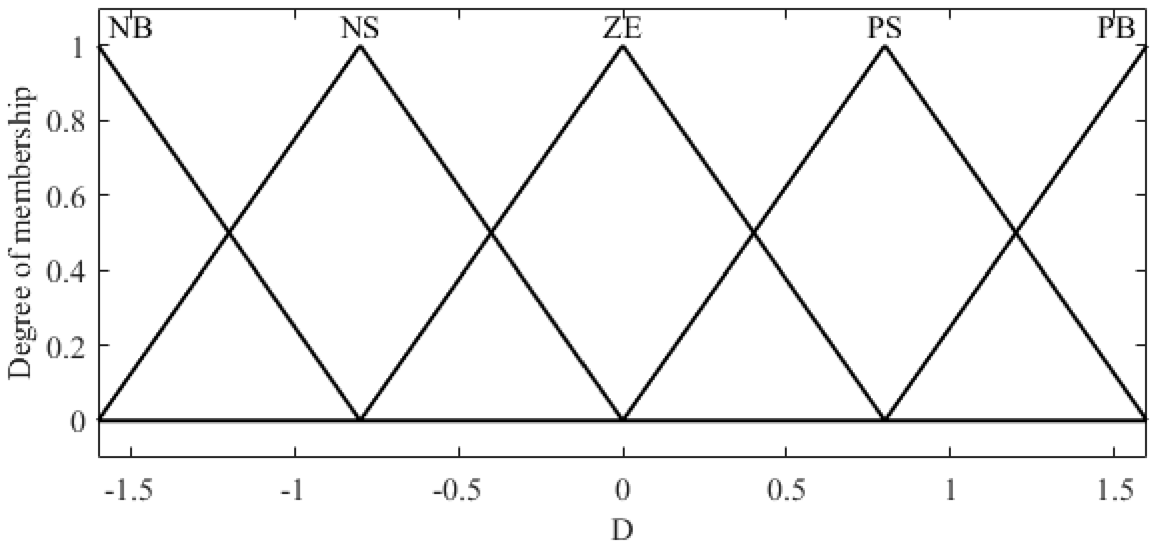

Figure 4.11. Output variable (D) membership function.

The inference rules, which may be divided into two parts: the rule base and the inference engine, constitute the second stage. Based on a set of input values, the fuzzy processor now employs linguistic rules to decide which control action should take place. The rule base is a collection of if-then rules that includes all the data for the controlled parameters and is set in accordance with professional expertise and operation system control.

There are 25 rules in the fuzzy logic algorithm that are used, and they are listed in Table 4.1. The inference engine converts the rule base into a fuzzy linguistic output with the aim of reaching a logical conclusion based on the fuzzy rule configuration. The fuzzy inference technique employed in the present study is Mandani's technique (E. Matagne et al, 2012)

(Dilovan Haji, et al., 2018). This stage produces a fuzzy output value that has been modified for each type of required action. The next phase, known as defuzzification, entails changing the fuzzy output values by their membership function to produce Crisp Outputs.

Table 4.1. FLC rule base.

E \ CE	NB	NS	ZE	PS	PB
NB	PB	PS	NB	NS	NS
NS	PS	PS	NB	NS	NS
ZE	NS	NS	PB	PB	PB
PS	NS	PB	PS	NB	PB
PB	NB	NB	PB	PS	PB

Defuzzification: The center of gravity approach is the defuzzification technique utilized for this system, producing the output duty cycle. When this method is used with the rule system that has already been provided, the duty cycle change is determined using the results of Equation (4.7).

$$\Delta D = \frac{\sum_{j=1}^{N} \mu \Delta D_j - \Delta D_j}{\sum_{j=1}^{N} \Delta D_j} \tag{4.7}$$

In order to modify the duty cycle value in accordance with the requirements of the system, the value of Equation (4.7) denotes the modification of the previous duty cycle. The boost converter's IGBT switch will be controlled by a PWM (Pulse Width Modulation) signal produced by the final duty cycle. It is anticipated that this controller will respond to changing environmental conditions more quickly and attain more stable parameters at steady state than the standard P&O, which has a set step size. This is because the change of duty cycle values is more flexible than the traditional P&O.

Figure 4.12 depicts the rule view, and it is useful to understand the real duty cycle ratio based on the two inputs. For instance, the graph shows that D is 0.97 when E and CE are, respectively, 0.0671 and 0.0421. This demonstrates one of the 25 rules, which states that D is PB when E is ZE and CE is ZE. Figure 4.13 also shows a 3D overview of the general control rules for the proposed FLC-based P&O MPPT controller. It has two inputs, E and CE, as well as a duty cycle ratio output, D. Based on the 25 rules implemented above, the input-output membership functions, and the figure is generated automatically.

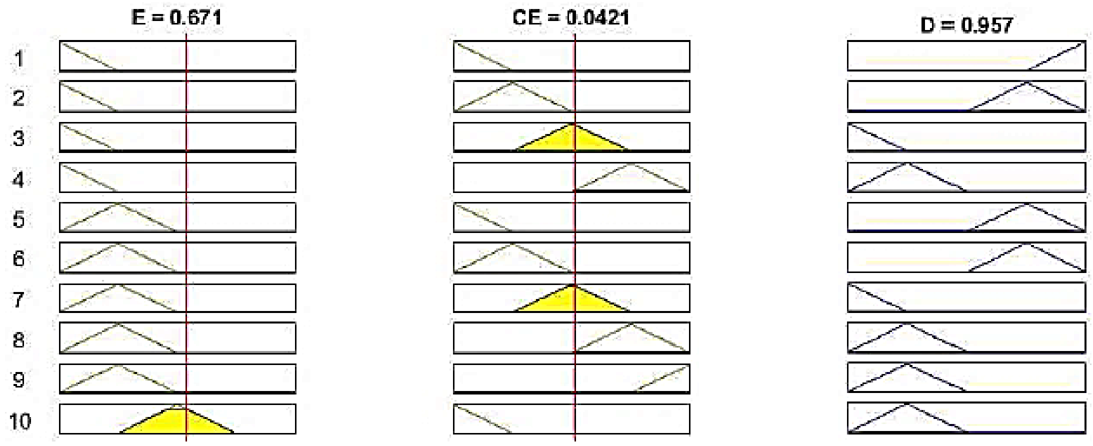

Figure 4.12. Rule views of the control algorithm

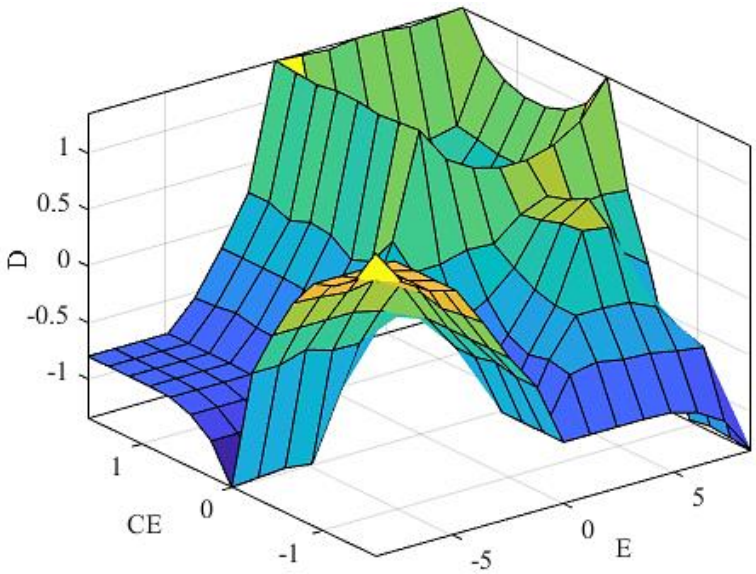

Figure 4.13. 3D surface view of the control rules.

Figure 4.14 displays the overall MATLAB/Simulink control system design. It also involves the application of rules in the fuzzy toolbox and the extraction of E and CE from the PV voltage and current using the P&O method. Additionally, a PWM generator is used to transform the fuzzy controller's duty ratio D-its output to PWM.

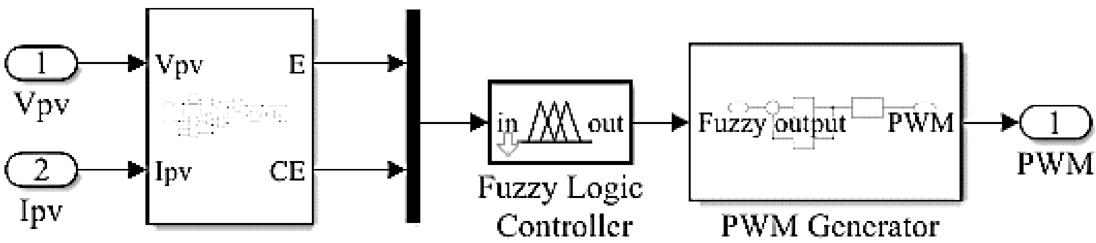

Figure 4.14. General Simulink design of the enhanced P&O using fuzzy logic controller.

CHAPTER FIVE

RESULT AND DISCUSSION

5.1. Chapter Overview

In this chapter the result and analysis of the proposed standalone PV MPPT control using Fuzzy enhanced P&O for pumping system is described. The system design includes a PV solar with a boost DC to DC converter, fuzzy enhanced P&O MPPT controller, three phase inverter, LC filter, DC load, and induction motor (AC motor). This all the design process is done in the previous consecutive two chapters.

A comparison analysis of the proposed MPPT controller with the conventional P&O algorithm has been done. Additionally, this chapter summarizes a cost analysis of the proposed system and its outcomes for the Koka agricultural activity.

5.2. Simulation Results

5.2.1. Simulation Result for DC Load

In this study, the system is simulated at the different solar irradiance values and at constant temperature condition. During simulation, the value of irradiance at 0W/m^2, 800W/m^2, 1000W/m^2, and 700W/m^2, and a constant temperature at 25^{o}C were considered. The total power generated from the PV array is 17kW which is achieved by using fuzzy enhanced P&O based MPPT algorithm which gives the most efficient stand-alone PV system. Hence, the load required 8.44kW and the generated power is enough to supply. Generally, the PV current, voltage, and power were obtained using the proposed controller employed for the stand-alone PV system.

Figure 5.1 to 5.3 shows the simulation result of photovoltaic array voltage, current, and power for the applied irradiance values and constant temperature. As it is shown that the PV array power has a direct relationship to solar irradiance. However, the solar irradiance is very low during the night and early morning. Therefore, the PV array power is almost reduced to zero.

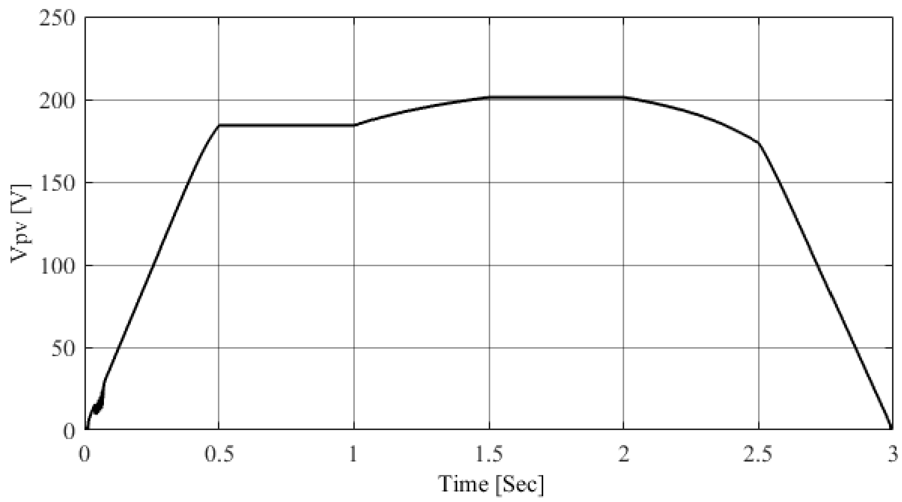

Figure 5.1. PV array output voltage

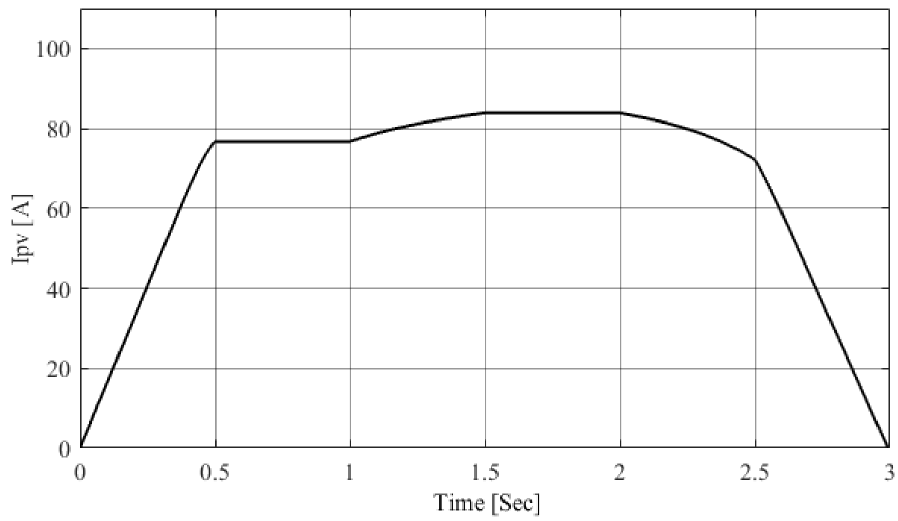

Figure 5.2. PV array output current

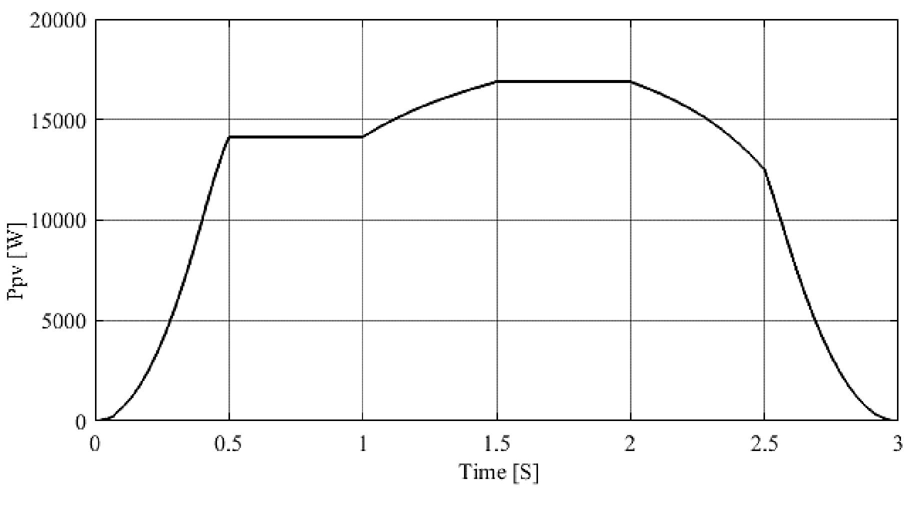

Figure 5.3. PV array output power

The output of the PV array is connected with a boost DC-DC converter. According to the design of the DC load assessment the maximum required voltage at 1000W/m^2 is 400v and its result is shown in Figure 5.4.

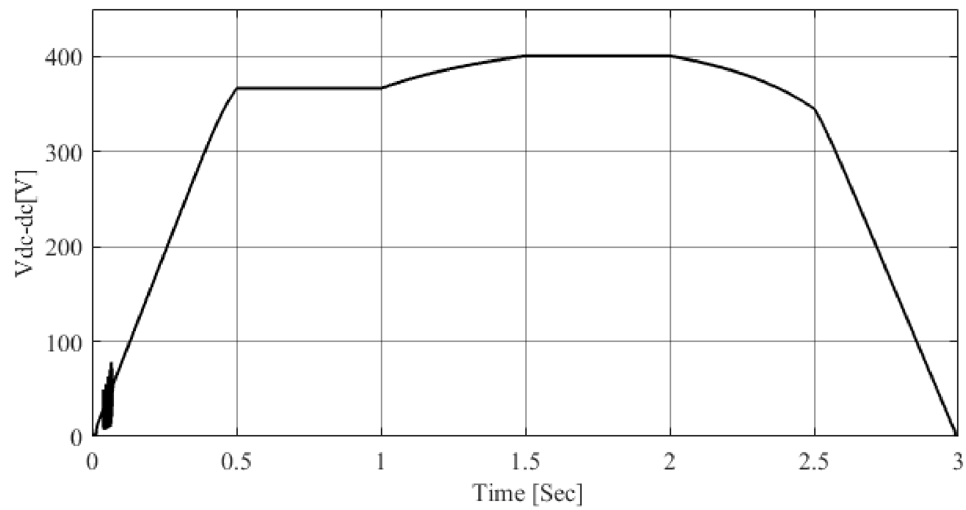

Figure 5.4. Output Voltage of DC-DC boost converter

The switching controller or MPPT controller as explained above is fuzzy enhanced P&O with PWM generator with a preset frequency 10kHz value. When the irradiance value is increasing the voltage and other output parameter is increasing and when the irradiance values are decreasing the parameters are decreasing and vice versa.

As explained in this section the different irradiance values considered for the simulation is shown in Figure 5.5.

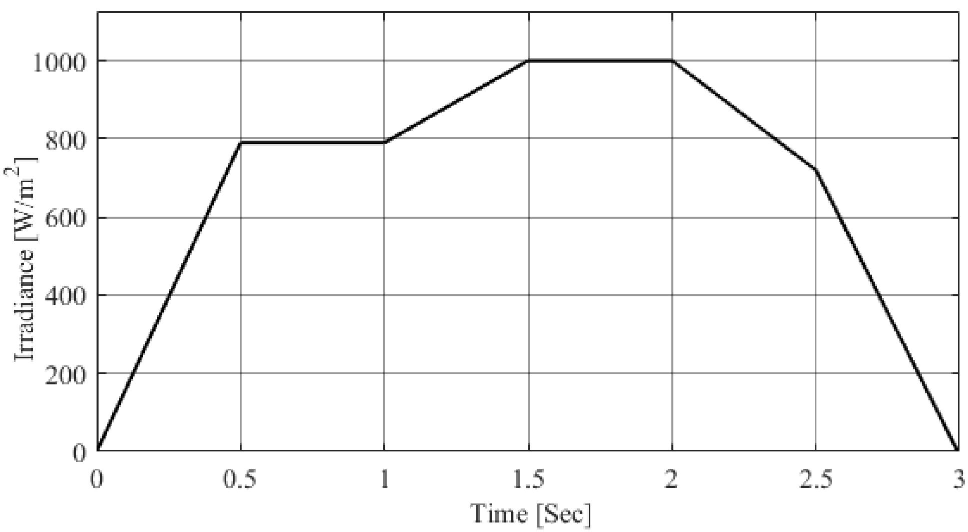

Figure 5.5. Different irradiance values considered for simulation

5.2.2. Simulation Result for AC Load

In this study the main aim is generating a power supply for induction motor water pumping system. Hence, usually the irradiance level in the winter season considered averagely 1000W/m^2 and it is considered for extracting the AC load results. When the motor is connected with the DC load the generated PV voltage is becoming around 220v and the total DC voltage at the output side of the converter is 1300v as can be seen in Figure 5.6 below at first result in read and black color lines respectively.

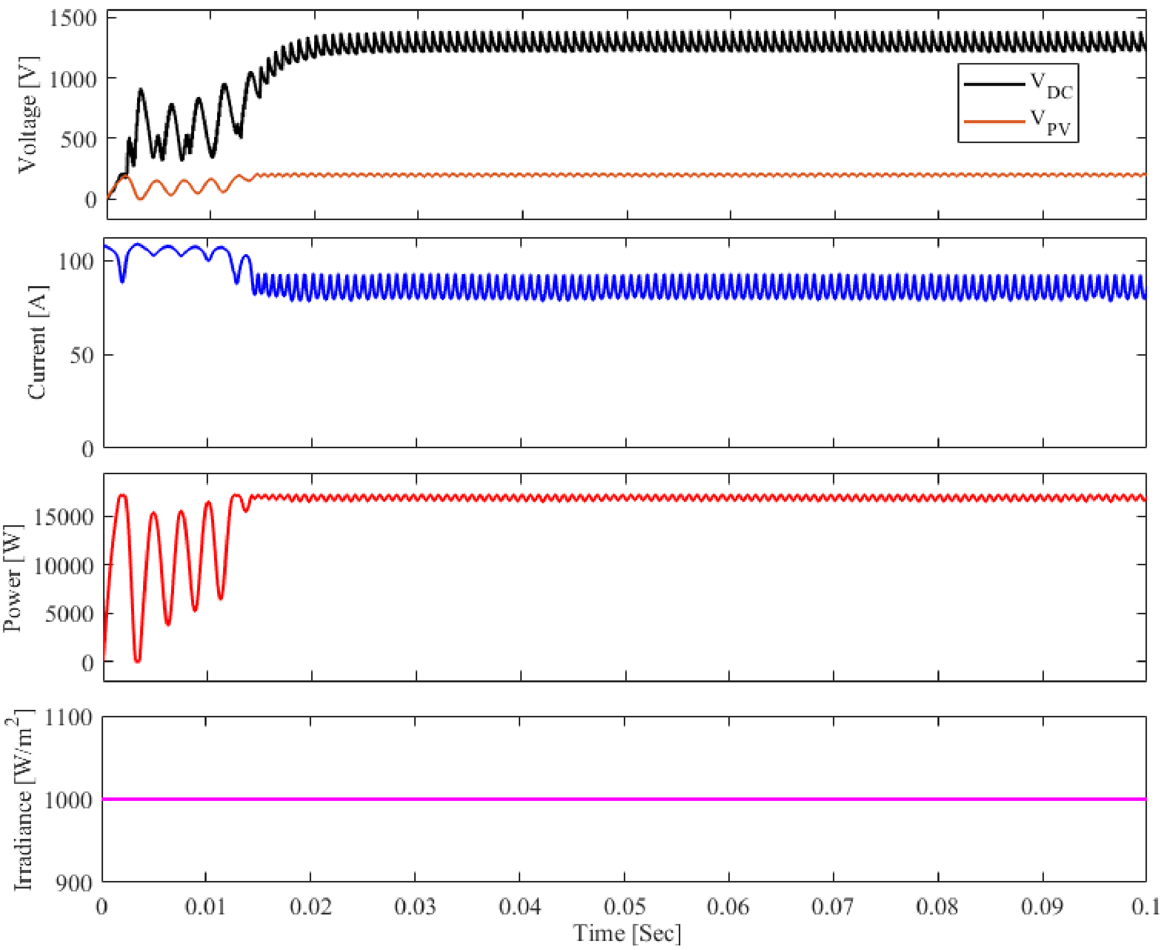

Figure 5.6. PV voltage, current, and power results when AC load is connected

Also, the generated PV current result is shown in the blue line which is around 85A. Since the PV power is analyzed based on the result of PV voltage and current and its result is 17kW as shown in the third result in red color. Hence, this output result is given to the three-phase two level (conventional) inverter.

In a similar way, a three-phase inverter is connected with induction motor for converting the DC parameter result to AC form. The voltage and current generated from PV side is converted in to three phase AC square wave as shown in Figure 5.7 and 5.8 and their magnitude values are 1300v and 21A respectively. Every square wave has harmonic and it needs some filtering techniques. Harmonics will generate unbalanced torque and vibration.

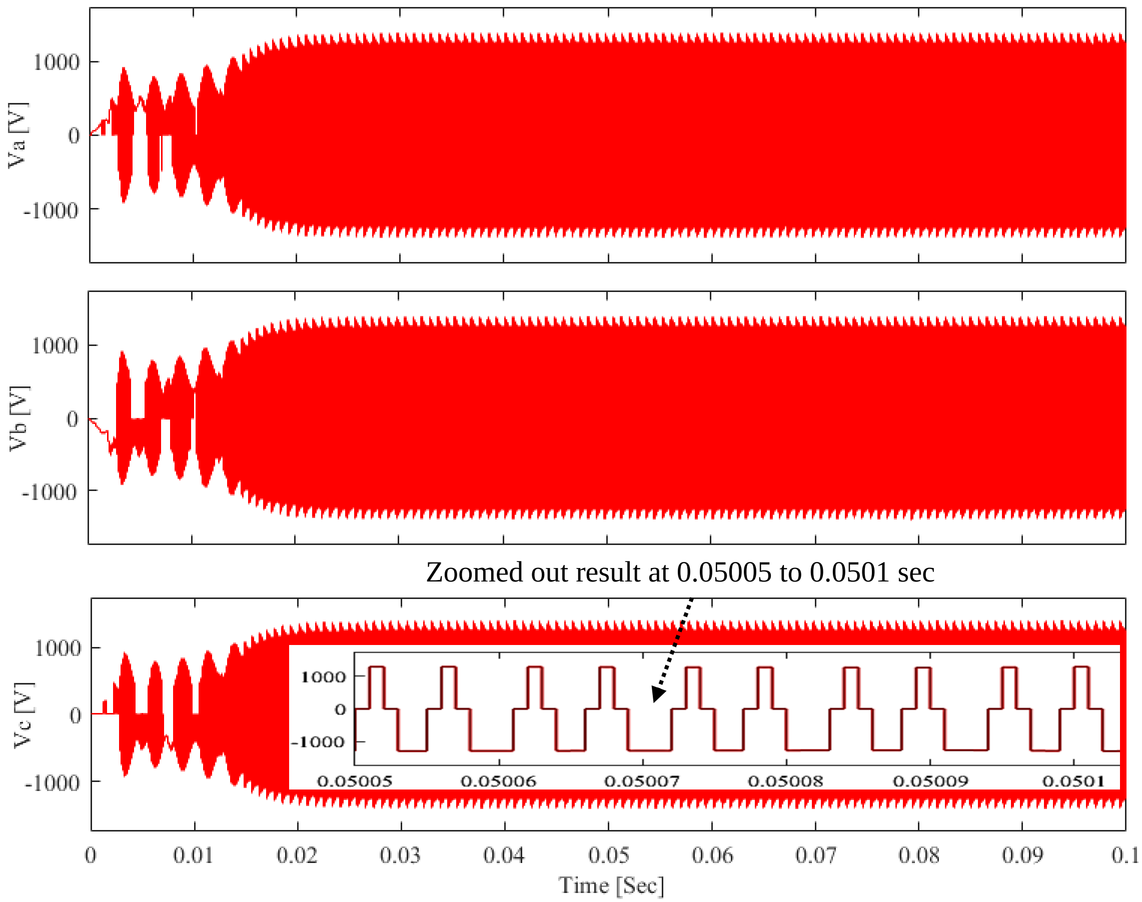

Figure 5.7. Three phase inverter output voltage

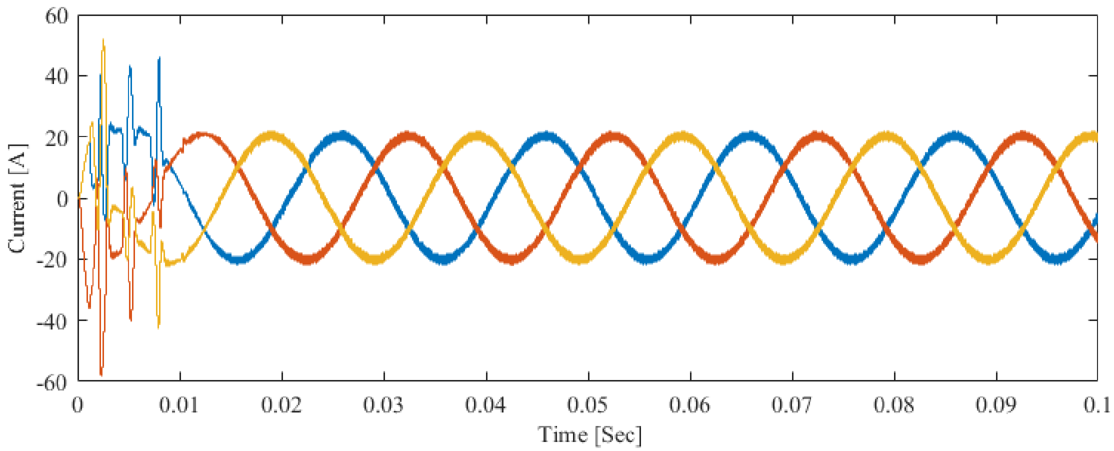

Figure 5.8. Three phase inverter output current

5.2.3. LC Filter Simulation Results

The final simulation element is the LC filter side. As explained in the previous chapter the LC filter is considered to minimize the harmonics generated by the three-phase conventional inverter. Hence, the motor requires 400v AC voltage, so the LC filter is designed to extract this voltage from the square wave inverter voltage. Accordingly, the three-phase sinusoidal voltage result is shown Figure 5.9 and its maximum peak voltage value is 400v as required except the distortion at starting between the time 0sec to 0.007sec.

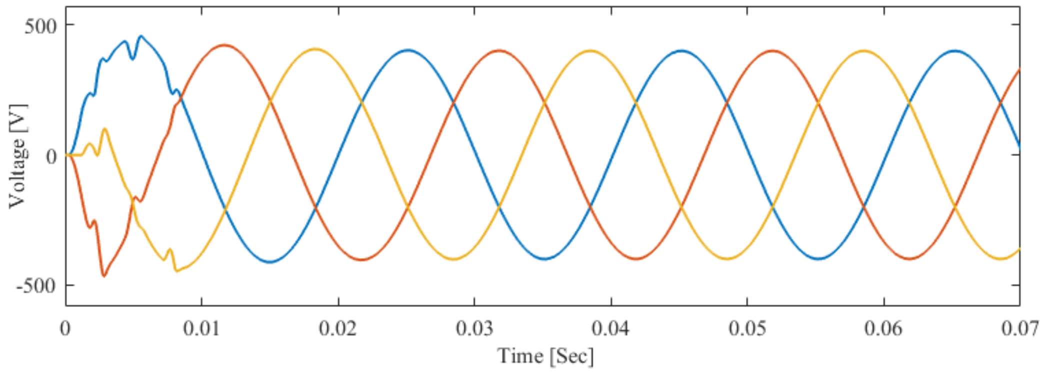

Figure 5.9. Three phase load voltage at the LC filter side

Moreover, the LC filter three-phase current also shown in Figure 5.10 and its maximum peak value is approximately 21A. In the same reason the current also has a distortion around starting time as the same with voltage shown in Figure 5.9 above.

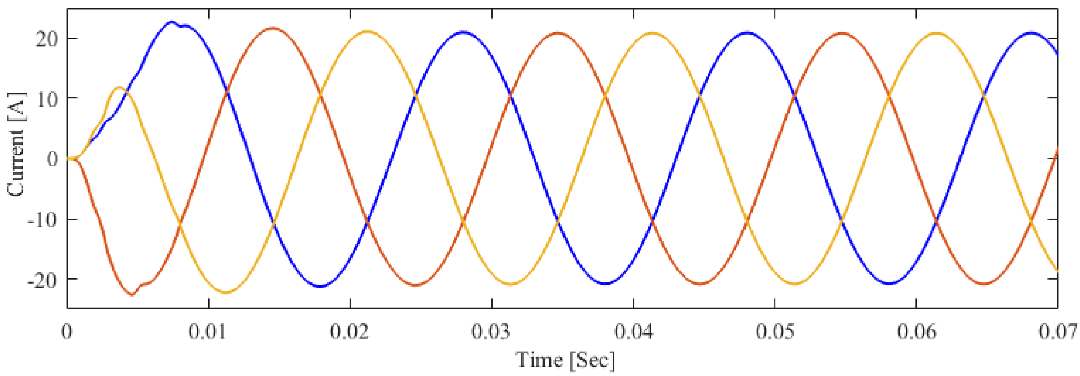

Figure 5.10. Three phase load current at the LC filter side

In addition, the motor is simulated at the required pump load and the motor three phase real power is shown in Figure 5.11. Its peak value is 6.4kW as shown in the result and in the same way the result has some distortion at starting like current and voltage results.

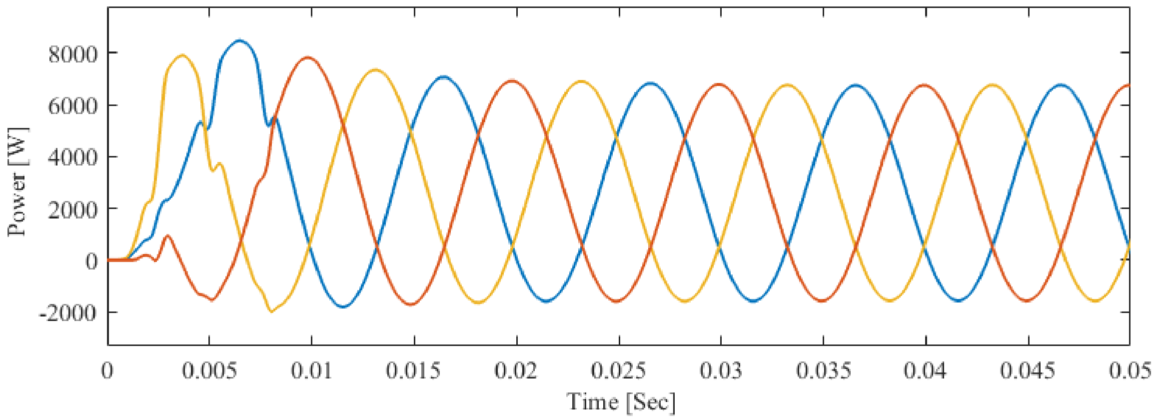

Figure 5.11. Three phase load power at the LC filter side

5.3. Discussion of the Results

Discussion of the results has been analyzed in this section. The discussion is based on two criteria. Firstly, the discussion is made based on the proposed Fuzzy enhanced P&O and the conventional P&O MPPT controller's result. And the other discussion is done according to the THD results on the proposed controller.

5.3.1. Discussion of Results on Fuzzy-P&O and conventional P&O MPPT

A DC-DC boost converter output voltage based on the fuzzy enhanced P&O and the conventional P&O controller is shown in Figure 5.12.

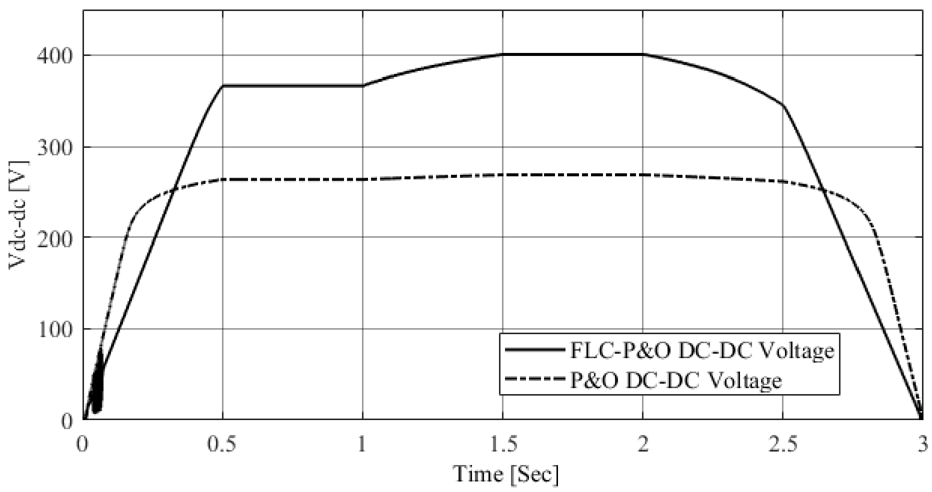

Figure 5.12. DC-DC converter voltage results on both controllers

As can been seen from the result the output voltage based on the fuzzy enhanced is tracking the DC link depending on the irradiance levels. Usually when the irradiance is variable there will be different local maxima and one global maximum value on the PV characteristics curve. Accordingly, the voltage at 1000W/m^2 is 400v as required and has different value as irradiance varies. As a result, the proposed controller usually tracks every maximum point as irradiance varies. But the output voltage result based on the conventional P&O is maximum of 250v in both PV voltage and DC-DC boost output voltage. As explained in the statement of the problems usually the conventional P&O MPPT controller tracks local maxima and there is no a chance to track the global maximum.

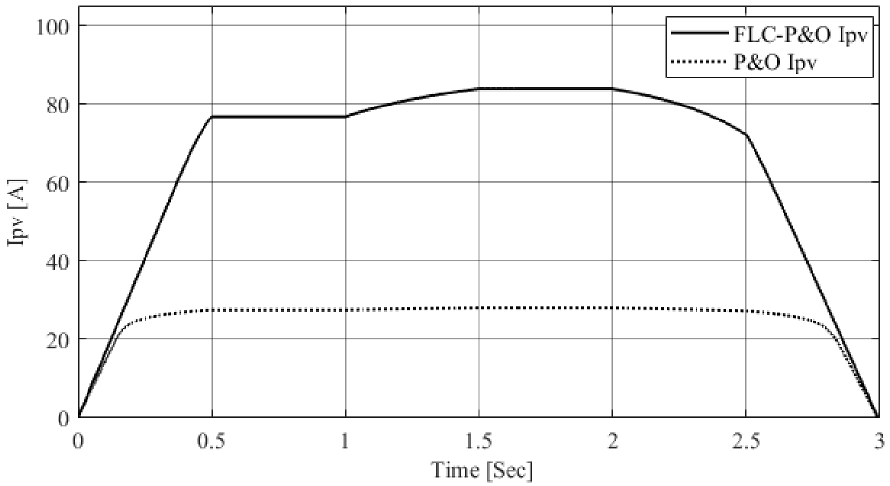

Figure 5.13. DC-DC converter current results on both controllers

Moreover, in the same way the current analysis also has the same explanation as voltage results. Its current result at 1000W/m^2 when Fuzzy-P&O considered is 85A but when the P&O considered the maximum current is 20A as shown in Figure 5.13.

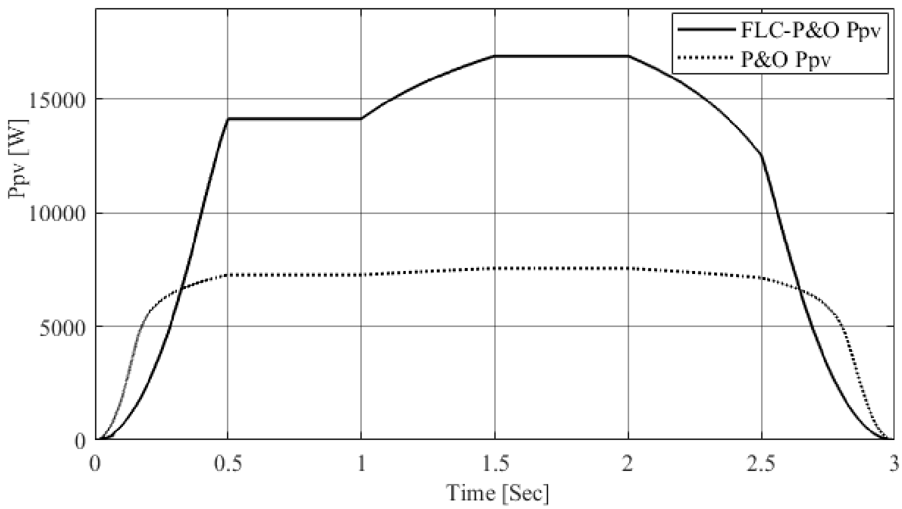

Figure 5.14. DC-DC converter power results on both controllers

The same is true for the PV power result shown in Figure 5.14. The output power when the proposed controller is applied 17kW at 1000W/m^2 and has different values as irradiance values. Also, the P&O based output power has shown in the figure and its maximum value is around 8kW. In all cases, the proposed controller has better results and can be applied for practical implementations.

5.3.2. THD Result Discussions

As explained in the previous sections the main disadvantage of the three-phase inverter is the harmonic distortions. In order to minimize this effect an LC filter is applied and the result THD is explained before and after filtering. Figure 5.15 is explaining the result of inverter phase-A current and its THD value is shown in Figure 5.16. Its fundamental magnitude at 50Hz and switching frequency of 10kHz is 21.7A and its THD is 53.54% and this shows the current is highly distorted.

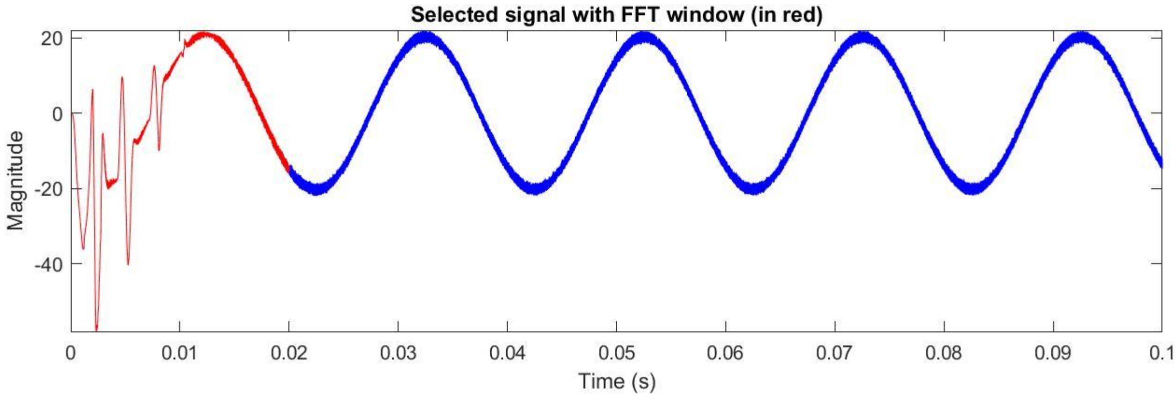

Figure 5.15. Phase A inverter output current

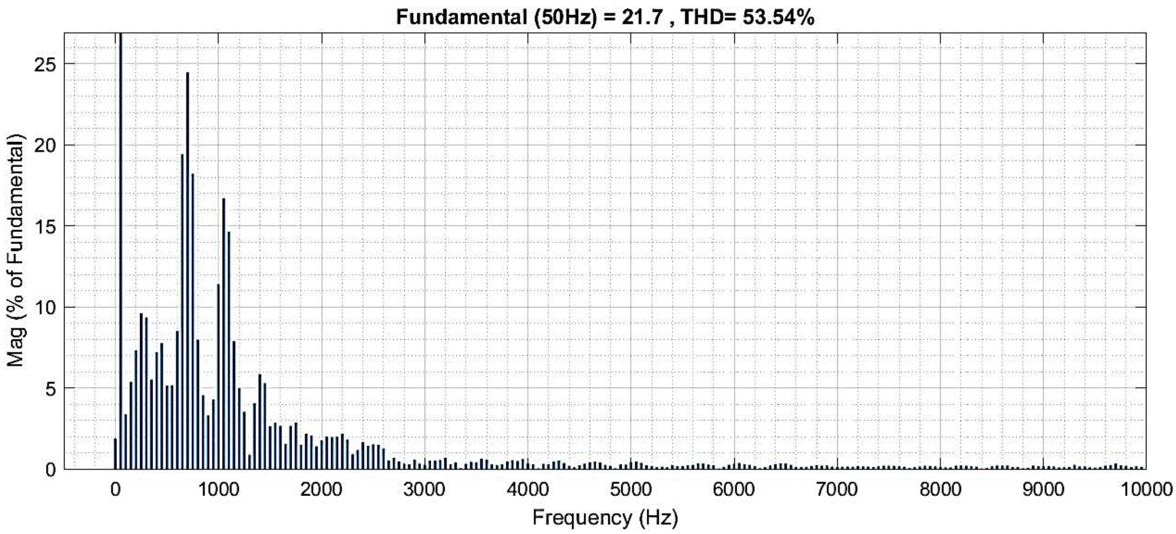

Figure 5.16. Phase A inverter output current THD result

After applying the LC filter, the THD value is analyzed as shown in Figure 5.17 and 5.18. The filtered Phase-A current at the fundamental current is shown Figure 5.17. which is pure sinusoidal except at starting has some distortion for a very small-time durations as explained in the previous section.

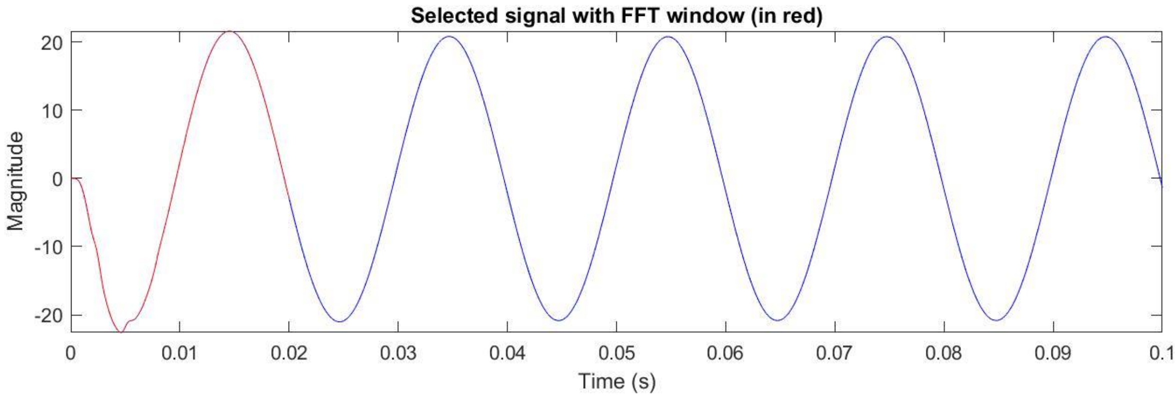

Figure 5.17. Phase-A LC filtered current

Its fundamental magnitude at 50Hz and switching frequency of 10kHz is 20.85A and its THD is 13.56% and this shows the current harmonics is minimized from the inverter side.

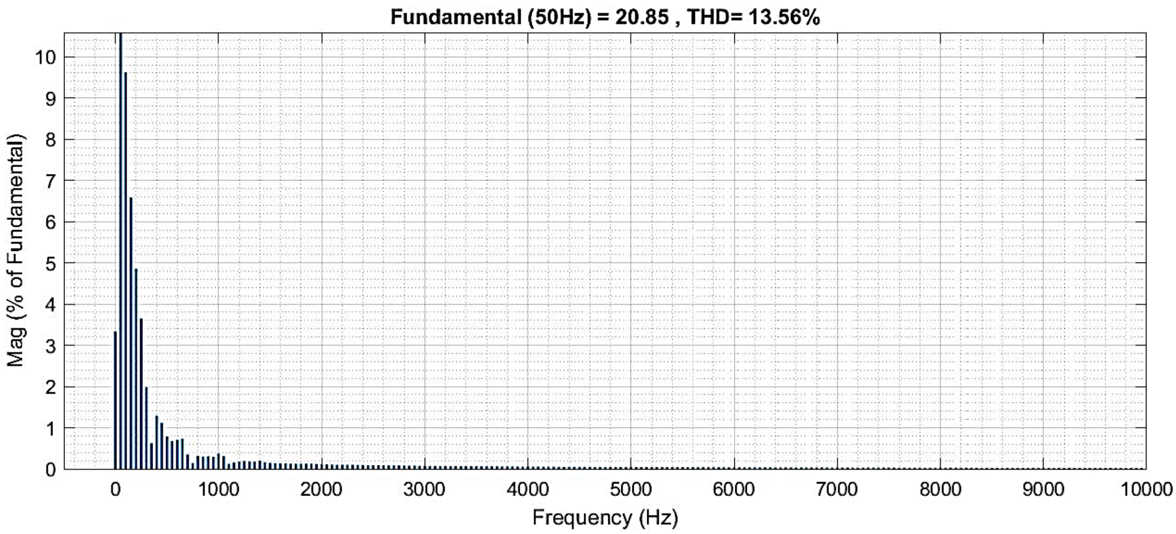

Figure 5.18. Phase-A LC filtered current THD result

In general, the THD is minimized from the 53.54% to 13.56% which is almost 40% is minimized. But, internationally 5% THD is required and this can be achieved by using multilevel inverters.

The design was considered to have 5% current harmonics, however from the result 13.56% is achieved. To achieve the 5% harmonics further investigations has to be considered. One of the well-known methods is using multilevel inverter than the two-level conventional inverter. When applying the multilevel inverter, the fundamental output current will be increased and inversely the harmonics content will be decreased. The other technique is applying different PWM techniques and might reduce the harmonics to some extent. In all cases the complexity and investment cost will be high as compared to the conventional two-level inverter. Also, for the applications like pumping no need to further investigations of harmonics reduction this is because of the motor is working in constant speed application.

CHAPTER SIX

CONCLUSION AND RECOMMENDATIONS

6.1. Conclusion

A stand-alone PV control system which consists of PV arrays, DC-DC boost converter, three phase inverter, LC filter, and Induction motor have been discussed in this study to achieve the power demand for the pumping application. Also, the mathematical cost analysis has been done for the proposed system application where electricity from the EEU does not satisfy the demand of the community as EEU not reached to the remote area.

In different aspects of the standalone PV proposed system such as sizing, modeling, controlling, and analysis of system components were discussed. For analyzing the system in all sections, the components were analyzed mathematically. Its different components and overall PV array system were modeled using MATLAB/Simulink. Based on its mathematical modeling, the appropriate sizes of a standalone PV system elements were applied and the models are simulated.

A fuzzy enhanced P&O MPPT controller is applied for the proposed system and a DC-link voltage is regulated at 400V. As per the analysis of the system the generated power were more than the power demand of the load and this was proved in the result and analysis sections. Hence for comparison purpose the conventional P&O and the fuzzy enhanced P&O MPPT control algorithms were implemented. Accordingly, the proposed control system results better results than the conventional one. Moreover, the THD analysis has been done before and after applying LC filter. As a result, the THD result at the inverter side is 53.54% which has more harmonic signals. After applying the LC filter, the THD result was found to be 13.56% and approximately 40% was reduced.

The NPC and COE were $128,155.05 and $0.20 respectively which is, reliable and efficient. Generally, the proposed standalone PV system was cost effective as compared with the current price of the COE of Ethiopian Electric Utility payment.

In general, the result of the proposed system based on the proposed controller was better result and can be applied to the real time scenario.

6.2. Recommendations

Nowadays, renewable energy is very vital for different activities in human needs. In Ethiopia mainly the urban areas get its energy from hydropower generation. Therefore, to improve energy imbalance between the urban and rural areas renewable energy like solar is required. Especially, in Koka the water resource is highly available however the people living there are not use it appropriately. Irrigation in the winter season is very necessary to cultivate crops twice in a year and this leads for economic development of the nation.

Implementations of this study will improve the problems regarding winter season crop cultivation. So, the representatives of government officials should get involved in providing financial support for procurement of proposed system components and make it a popular energy source in the place since as there is no operational cost. Moreover, it can be applicable for the energy problems in health centers, commercial, and buildings in remote areas.

Moreover, in order to improve the THD values it will be better if multilevel inverter is applied for the proposed system in order to make below 5%. However, this will lead additional cost and complexity in the controller design.

REFERENCE

A. Nasir, "Design, Simulation and Analysis of Photovoltaic Water Pumping System for Irrigation of Potato Farm at Gerenbo," 2016.

A. Omar et al., "Modeling of a maximum power point tracker for a stand-alone photovoltaic system using MATLAB/Simulink," *International Journal of Low-Carbon Technologies*, no. 9, p. pp 195–201, 2014.

A. September, "Renewable Energy Water Pumping System," July 2004.

A. Tadessie, "Feasibility Study of Small Hydro/PV/Wind Hybrid System for Off-Grid Rural Electrification in Ethiopia," *Addis Ababa Institute of Technology Master's Thesis, Power Engineering Stream,* May 2011.

Abdullah M. Noman, et al. (2012), A Fuzzy Logic Control Method for MPPT of PV Systems, Electrical Engineering Department, Sustainable Energy Technologies Center, King Saud University, IEEE, 2012

B. Alsayid, "Modeling and Simulation of Photovoltaic Cell/Module/Array with Two-Diode Model," *International Journal of Computer Technology and Electronics Engineering,* Vols. Volume 1, no. Issue 3, June 2012.

B. V. Emmanuel, "Solar PV system sizing," *University of Nairobi*, 2009.

Benghanem, M. and e. al., "Performance of Solar Water Pumping System Using Helical Pump for a Deep Well:" *Energy Conversion and Management*, p. 65, 2013.

Bereket Fola, "Design and Analysis of Solar Powered Multilevel Inverter Fed Induction Motor Drive for Water Pumping Application (Case Study on Koka in Adama, South-East Ethiopia)", *Adama Science and Technology University Master's Thesis, Power Electronics*, September, 2020

D. A. Mousse, A. Saudi, A. Beta and a. G. Asher, "Photovoltaic Pumping Systems Technologies Trends," *Lahr's Journal, ISSN*, pp. 127-150, June 2013.

D. K. Sharma, "Analysis of the Effect of Fill Factor on the Efficiency of Solar PV System for Improved Design of MPPT," *in Department of Electronics & Comm. Engg, Udaipur INDIA*, 2014.

Dilovan Haji, et al., (2018), Fuzzy and P&O Based MPPT Controllers under Different Conditions, 7th International Conference on Renewable Energy Research and Applications, Paris France, Oct.14-17, 2018

E. Matagne et al., Optimization of Photovoltaic Power Systems, ISSN, 2012.

E. Muliadi, "PV Water Pumping with A Peak Power Tracker Using Simple Six-Step Square Wave Inverter," *IEEE Trans. Ind*. Appl., Vols. 33, No. 3, pp. 714-721, May, 1997

Emmanuel Kwaku Anto et al., "PID-based P&O MPPT Controller for Off grid PV Systems Using Ziegler-Nichols Tuning Method to Step, Ramp and Impulse Inputs," *Journal of Multidisciplinary Engineering Science Studies*, vol. Vol. 2, no. Issue 7, 2016.

Energy, Information, Administration and (US)., Annual Energy Review 2011., *Government Printing Office* 2012.

Ethiopian Electrical Power in December 2016.

G. E. Ahmad, "Photovoltaic Powered Rural Zone Family House in Egypt," *Renewable Energy*, vol. 26, pp. 379-390, 2019.

Guide, The Kyocera Solar Inc. Solar Water Pump Applications Available from: http:/www.kyocerasolar.com.

H. Mark, Stand-Alone Solar Electric Systems, 2010.

H. Raffel, "Realization of a Quasi Direct Converter by a High Dynamic DC Link Voltage Regulator," *PhD Thesis, University of Bremen*, 2003.

Hussein Selman, N. (2016). Comparison Between Perturb & Observe, Incremental Conductance and Fuzzy Logic MPPT Techniques at Different Weather Conditions. International Journal of Innovative Research in Science, Engineering and

I. Sefa and I. Altin, "Grid Interactive Photovoltaic Inverters-a Review," *JFac Eng Archit Gazi Univ*, pp. 24(3):409-24, 2017.

I. Sefa, M. Demirtas and I. Colak, "Applications of One Axis Sun Tracking System," *Energy Convers Manage*, pp. 50:2709-18, 2015.

J. Grant, "Design and Simulation of a DC Microgrid for a Small Island in Belize," *Sustainable Energy Engineering, Iceland School of Energy*, 2018.

J. S. Lai and F. Z. Peng, "Multilevel Converters- A New Breed of Power Converters," *IEEE Trans. Ind*. Applicat., vol. 32, pp. 509-517, May/June 2013.

J. Uboori et al., "Stand-Alone Photovoltaic System," Energy Sci. & Tech., vol. vol.6, 2016.

K. I. Mirza Mursalin Iqbal, "Design and Simulation of A PV System with Battery Storage Using Bidirectional DC-DC Converter Using MATLAB Simulink," *IJSTR*, Vols. 6, no. ISSUE 07, pp. pp 2277-8616, JULY 2017.

M. Ababa, "Matching Induction Motors to PVG for Maximum Power Transfer," *Elsevier-Desalination*, pp. 31-38, 2014.

M. B. Kumar, " Modeling and Control of PV/Wind," Halmstad University, 2017.

M. Martino, "Intelligent Control for Distributed System," 2012.

M. Parimita, M. Tariq and K. Mohan, Solar Photovoltaic System Applications, 2016.

Mishra, P., & Maheshwari, R. (2020). Design, analysis, and impacts of sinusoidal LC filter on pulse width modulated inverter fed-induction motor drive. *IEEE Transactions on Industrial Electronics,* 67(4), 2678-2688.

Online1, https://customenergy.com Most popular types of solar panels explained, [Accessed 11, 02, 2023].

Online2, https://www.google.com/imgres the most common types of solar panel, [Accessed 11, 02, 2023]

Online3, http://www.energybc.ca/cache/solarpv/www.cetonline.org/Renewables/PV, [Accessed 11, 02, 2023].

Online4, https://core.ac.uk/download/pdf/61802295. DC to DC converter pdf, [Accessed 11, 02, 2023].

Online5, "https://www.google.com/search?q Solar Panels Specifications," [Accessed: 11, 04 2023].

Panels1, the Planet's most Powerful Available from: http://us.sunpowercorp.com/homes/sunpoweradvantage/more-electricity [Accessed 11 02 2021].

Panels2, the Photovoltaic Panels Work Available from: http:/www.Irc.rpi.edu/programs/nlpip/lightingAnswers/photovoltaic/04-photovoltaic-panels-work.asp

[Accessed 11, 02, 2023].

Photovoltaic Powered Water Pumping Systems: Design and Optimization of an Irrigation System, Maria Ines Cardoso Bexiga 2014.

Pump selection handbook-Carson Ca, 2011

Renewable energy, Design guide and catalog, Shewin Electric, 2008-2009.

S. D. Gon, "Design of a Standalone Photovoltaic System for a Typical Household around Dessie City-Ethiopia," *American Journal of Electrical and Electronic Engineering,* Vols. Vol. 7, No. 1, 1-7, 2019.

T. El Shenawy et al, “Design and Optimization of Stand-alone PV System for Egyptian Rural Communities," *International Journal of Applied Engineering Research,* Vols. Volume 12, Number 20, pp. pp. 10433-10446, (2017).

U. Report, "Eastern and Southern Africa Available from: https://www.unicef.org".

V. Quaschning, Renewable Energy and Climate Change, *John Wiley and Sons*, 2010.

Y. S. Mohammed Kharrich and Mohamed Akherraz, "Optimal Sizing of an Islanded Microgrid based on PV, Wind and Battery Energy Storage System," *International Conference on Automation, Control Engineering and Computer Science,* vol. Vol.20, pp. pp.71 - 76, 2017.

Y. Zhang, "Control and Power Management of Photovoltaic Systems with Plug-in Hybrid Electric Vehicles as Energy Storage," *University of Tasmania,* October 2017.

APPENDIX

Appendix A: Overall MATLAB Simulink Model

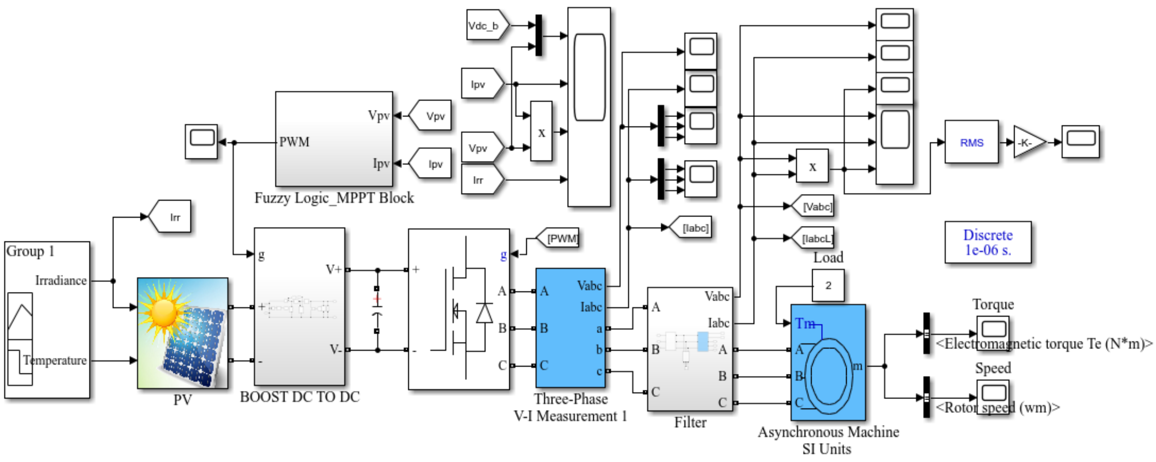

Appendix A.1: Fuzzy P&O algorithm implementation

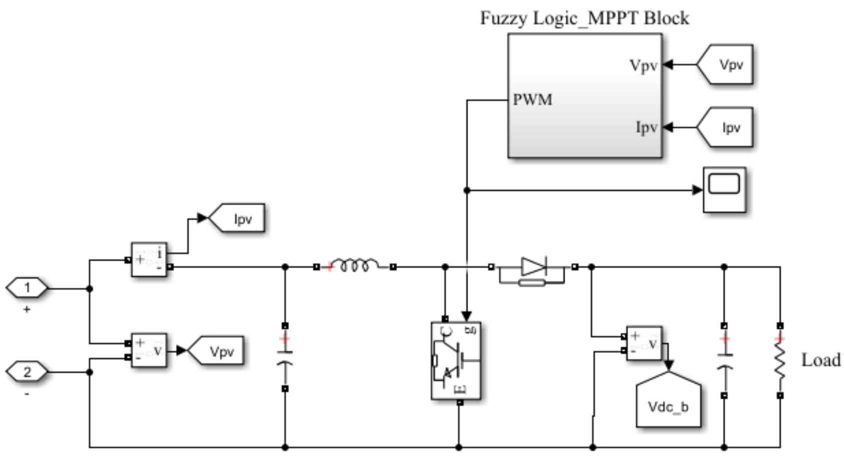

Appendix A.2: Implementations of P&O algorithm

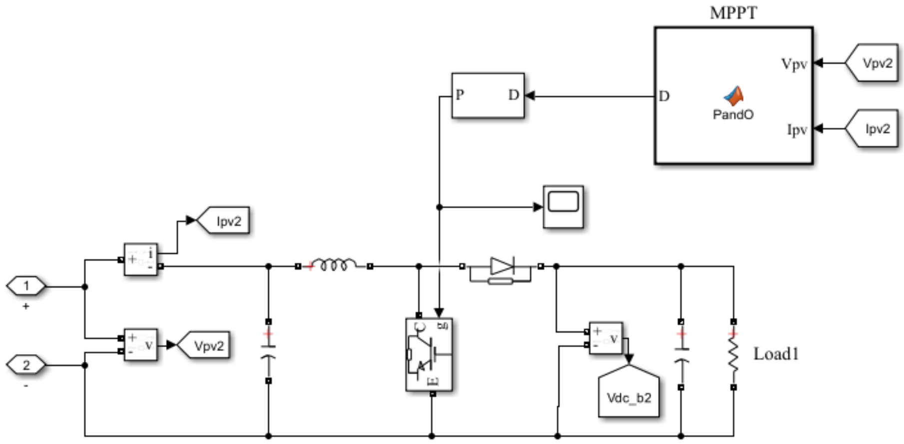

Appendix A.3: Solar PV design in simulink

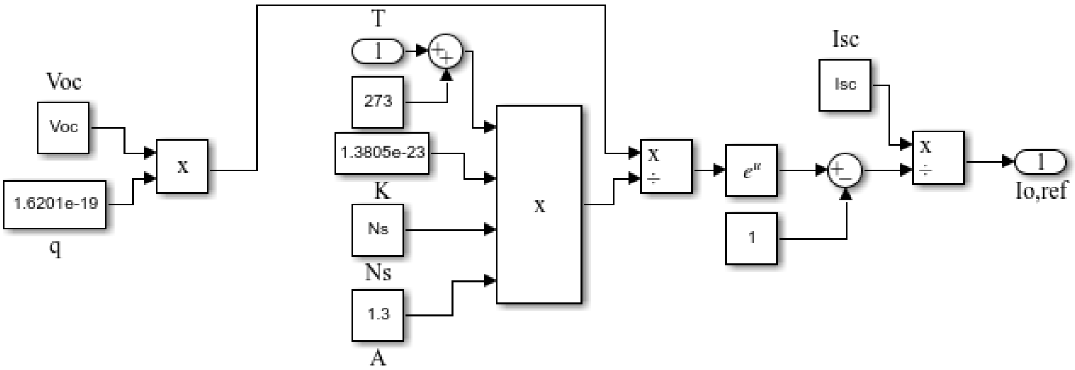

Modeling of light generated current

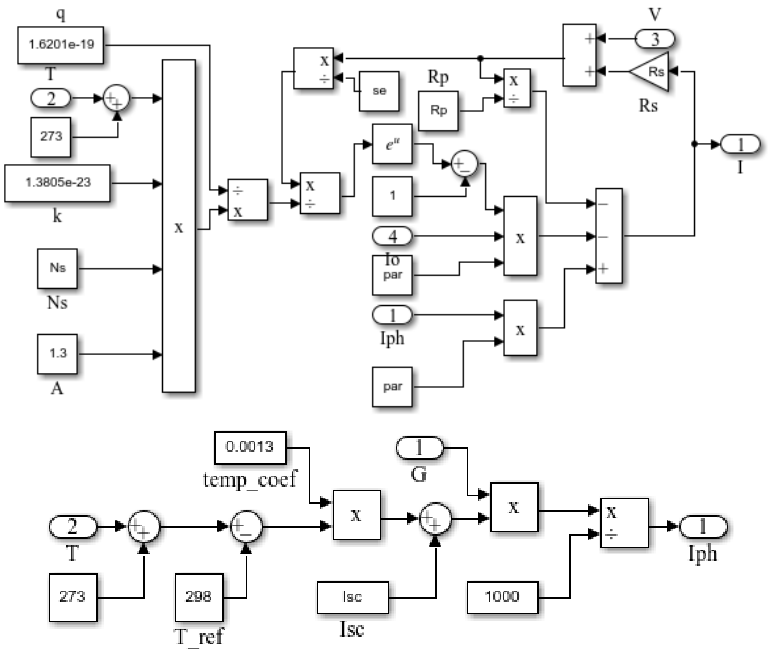

Block diagram of saturation current

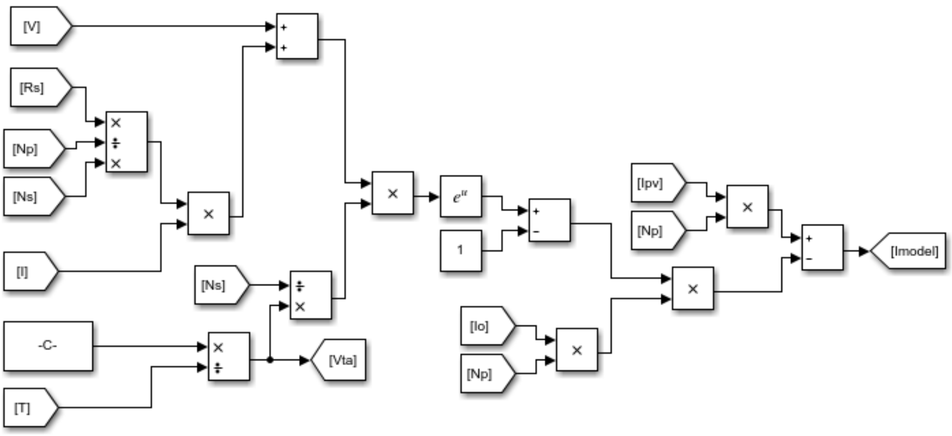

Simulink diagram of the photovoltaic current

Appendix B: Solar module specification

ELECTRICAL SPECIFICATIONS

*STC : Irradiance 1000W/m^2, AM1.5 spectrum, module temperature 25ºC

Model Type	CSS-MSP-250M-60
Peak power (Pmax)	250W
Cell Efficiency	17.24%
Maximum power voltage (Vmp)	30.8V
Maximum power current (Imp)	7.79A
Open circuit voltage (Voc)	37.4V
Short circuit current (Isc)	8.49A
Power Tolerance	±3%
Maximum system voltage	1000V
Series fuse rating (A)	15
Number of bypass diode	3/6

TEMPERATURE COEFFICIENTS

Current Temperature Coefficient α(Isc)	0.03%/ºC
Voltage Temperature Coefficient β(Voc)	- 0.32%/ºC
Power Temperature Coefficient γ(Pmax)	-0.42%/ºC

MECHANICAL CHARACTERISTICS

Dimensions:	1640 x 990 x 40mm (64.57 x 38.98 x 1.58 inch)
Weight:	19.8 kg (43.56 lbs)
Solar Cells:	60 cells in series (6x10)
Construction:	High-transmission low-iron tempered glass, EVA, TPT
Frame:	Anodized aluminum is mainly for improving corrosion resistance. Color: silver